Title

Weak palaeointensity results over a Pliocene volcanic sequence from Lesser Caucasus (Georgia): transitional record or time averaged field?

Journal
Geophysical Journal International, 220(3)

ISSN
0956-540X

Authors
Sánchez-Moreno, Elisa M
Calvo-Rathert, Manuel
Goguitchaichvili, Avto
et al.

Publication Date
2020-03-01

DOI
10.1093/gji/ggz533

Peer reviewed

Weak paleointensity results over a Pliocene volcanic sequence from Lesser Caucasus (Georgia): Transitional record or time averaged field?

Elisa M. Sánchez-Moreno[1,*], Manuel Calvo-Rathert[1,2], Avto Goguitchaichvili[3], Lisa Tauxe[4], George T. Vashakidze[5], Vladimir A. Lebedev[6]

[1]Departamento de Física, EPS Campus Rio Vena – Universidad de Burgos, Av. Cantabria, s/n, 09006 Burgos, Spain.
[2]Hawaii Institute of Geophysics and Planetology, University of Hawaii at Manoa, Honolulu, HI, United States
[3]Laboratorio Interinstitucional de Magnetismo Natural, Instituto de Geofísica Unidad Michoacán, UNAM – Campus Morelia, 58990 Morelia, México.
[4]Scripps Institution of Oceanography, University of California - San Diego, La Jolla, CA 92093-0220, USA.
[5]Alexandre Janelidze Institute of Geology – Ivane Javakhishvili Tbilisi State University, 1/9 M. Alexidze str., 0171 Tbilisi, Georgia.
[6]Institute of Geology of Ore Deposits, Petrography, Mineralogy and Geochemistry – Russian Academy of Sciences (IGEM RAS), Staromonetny per., 35, 119017 Moscow, Russia.

*Corresponding author, Elisa M. Sánchez-Moreno: emsanchez@ubu.es

Key words: Paleointensity; lava flow sequence; Pliocene; transitional record; weak time-averaged field

Abstract

A paleointensity study has been carried out on a Pliocene sequence of 20 consecutive lava flows where previous directional results seem to reflect anomalous behavior of the Earth's magnetic field (EMF), which can be explained by a polarity transition record or non-averaged paleosecular variation or both. Here, we perform a total of 55 paleointensity determinations using the original Thellier-Thellier method and 100 with the IZZI method. We assess the performance of our selection criteria using a set of strict threshold values applied to a set of test data whose TRMs were acquired in known fields. Absolute paleointensity determinations that passed our selection criteria were obtained on four specimens with the Thellier-Thellier method and on 41 specimens with the IZZI method. Application of reliability criteria at a site level yielded paleointensity results in eight of 20 studied lava flows. We obtained median values of VADM between 28.9 and 45.6 ZAm^2 for the reverse polarity lower Apnia section, while the normal polarity upper section displayed a single value of 54.6 ZAm^2. The low paleointensity values before a transitional direction lava flow and the higher value after it, suggest the common

behavior at the start of a polarity reversal and the recovery after it. However, an isolated record of a stable EMF, where the intensity is lower than the current for the same location (83.7 ZAm^2), cannot be discarded. Consequently, this interpretation would support a weak time-averaged field.

1. Introduction

The study of the Earth's magnetic field (EMF) characteristics and variations requires knowledge of both its direction and intensity. The direction of the ancient field can be measured directly because the magnetization recorded in a rock is usually parallel to the magnetizing field direction. Absolute paleointensity cannot be measured directly as the magnetic remanence is only proportional, but not equal to the ancient field intensity. The combined (directional and intensity) analysis of paleomagnetic results supplies new information for an enhanced understanding of the processes that occur in the outer core and control the geodynamo, the source of the fluctuations of the EMF (e.g. Barton, 1982; Johnson and Constable, 1996; McElhinny et al., 1996; Merrill et al., 1996; Carlut et al., 1999; Merrill and Mcfadden, 2003; Constable and Johnson, 2005; Harrison, 2007; Johnson et al., 2008; Glatzmaier and Coe, 2015; Tarduno et al., 2015; Smirnov et al., 2017; Lund, 2018).

Although so far several different paleointensity determination methods have been used, those based on the original Thellier method (Thellier and Thellier, 1959) are considered to be the most reliable ones, because they rely on a stringent physical basis. Nevertheless, absolute ancient field intensity data are scarcer than directional data, because they can only be obtained from materials in which the magnetization was acquired by a thermal mechanism, i.e. they have to carry a thermoremanent magnetization (TRM), as found in most volcanic rocks. In addition, in paleointensity determinations, in order to be successful, no magneto-chemical alteration of the remanence-carrying minerals may occur as a result of heating during the experiments, and the remanence should be ideally carried by single-domain grains (Thellier and Thellier, 1959). The success rate in paleointensity determinations is relatively low, and the currently available database shows a large degree of scatter – even for results from a single lava flow (e.g., Cromwell et al., 2015).

Consecutive lava flow sequences provide a succession of instantaneous field states of the EMF at the time of emission as recorded by a TRM, thus allowing the analysis of both directional and intensity EMF variations. Regarding stable EMF periods, several paleointensity studies performed during the last two decades have shown that average values of the virtual axial dipole moment (VADM) yield intensities of approximately half of the present-day value (current EMF strength ~80 ZAm^2) (e.g. Juárez et al., 1998; Juárez and Tauxe, 2000; Tauxe, 2006; Lawrence et al., 2009; Tauxe et al., 2013; Cromwell et al., 2015; Wang et al., 2015). Other studies, however, have yielded average VADM values during stable EMF periods which are near the present dipole moment (Heller et al., 2002; McFadden and McElhinny, 1982; Smirnov and Tarduno, 2003; Tanaka et al., 1995c; Valet et al., 2005). Knowledge about the characteristics of the EMF during anomalous periods like polarity reversals and geomagnetic excursions is even more limited, as the difficulty in finding records that cover the specific time period in which these events have occurred has limited the number of studies reported so far in comparison with those related to periods of a stable EMF (i.e. within normal or reverse polarity chrons).

This work focuses on the analysis of the paleointensities recorded in the basaltic flow sequence of Apnia (Djavakheti Highland, Southern Georgia), which has been dated by the $^{40}K/^{40}Ar$ method (Lebedev et al., 2008) yielding an age between 3.70 and 3.09 Ma. The paleomagnetic directions (Sánchez-Moreno et al., 2018) show, from bottom to top, 14 reverse polarity flows, followed by a transitional one and five normal polarity flows. Both mean poles of the normal and reverse populations disagree with the expected pole for the same age range. The virtual geomagnetic pole (VGP) scatter angle, with respect to the reference pole, in lower Apnia is 14.7°, matching the expected one (~15°-17° taken from Model G (McFadden et al., 1988) of paleosecular variation of lavas (PSVL) fits to data from the last 5 Ma from McElhinny and McFadden (1997) and Johnson et al. (2008). Despite Model G having been reviewed and its limitations for accurately estimate the PSV latitudinal dependence having been pointed out (Doubrovine et al., 2019), it remains fully descriptive of the EMF behavior during periods of stable polarity. Meanwhile in the upper sequence is VGP scatter yields a higher 21.3°, but its confidence interval spans the expected PSV scatter values. Directional results are inconsistent with stable EMF behavior and could indicate a polarity transition or a record of several transitions, according to the ages obtained. On the other hand, the mismatch with the expected pole and the high dispersion could be the result of paleosecular variation (PSV) that has not been averaged out. This second interpretation does not exclude the first one (Sanchez-Moreno et al., 2018). The paleointensity data obtained from this work could provide new information to accept or reject the interpretation of a polarity reversal (or composite) record. Previous paleomagnetic and paleointensity results obtained on Plio-Pleistocene basaltic sequences in the volcanic region of Djavakheti display reliable records of both stable and unstable magnetic field regimes (Calvo-Rathert et al., 2011; 2013; 2015; Camps et al., 1996; Goguitchaichvili et al., 2000, 2001, 2009). Despite these previous studies, directional and especially reliable, high quality paleointensity data in the Caucasus region are still scarce.

In the present study, two different paleointensity determination methods have been applied to the Apnia samples: The original Thellier method (TT) (Thellier and Thellier, 1959) and the IZZI method (Yu et al., 2004). As the aim of the study is obtaining reliable, high quality paleointensity data, especially strict selection criteria for successful determinations have been applied. We have used the set of quality criteria proposed by Cromwell et al. (2015), which was referred to as CCRIT by Tauxe et al. (2016), but we have divided the threshold values of the proposed criteria into two levels, with the goal of distinguishing two quality ranges. The first is called directly CCRIT, with threshold values similar to those of Tauxe et al. (2016). The second one, called RCRIT (Sánchez-Moreno, 2018), is a somewhat less stricter version of the first one, although still stricter than other sets of criteria and threshold values frequently used (e. g. Biggin et al., 2007; Kissel and Laj, 2004; Leonhardt et al., 2004; Tauxe et al., 2013).

2. Geological setting

The Apnia sequence (41°21'40"N, 43°16'02"E) was sampled in the volcanic Djavakheti Highland region, located in the central sector of the Lesser Caucasus (South Georgia) (Fig. 1.). This mountain range, included in the Alpine-Himalayan belt, is still being generated by the active collision of the Eurasian and Arabian plates. Within the so-called post-collision stage (late Miocene - Quaternary) (Adamia et al., 2011) different phases of volcanic activity took place (Lebedev et al., 2008a) in the Lesser Caucasus area: I) Terminal Miocene (~7.5 Ma), II) 3.7-1.8 Ma and III) Last 800 ka. The volcanism, which generated the materials under study, corresponds to the second phase. A large number of volcanic cones and fissure volcanoes owing to NW-SE and NE-SW extensional strike-slip structures, which also developed by the compressional regime (Avagyan et al., 2010), characterize this phase. The numerous resulting consecutive basic lava flows created the current Djavakheti and Armenian plateaus. They are known as Akhalkalaki Formation in the Djavakheti region (Maisuradze and Kuloshvili, 1999).

The Apnia sequence comprises 20 consecutive lava flows of calc-alkaline basalts and basaltic andesites, belonging to the Akhalkalaki Formation, that were sampled from top (AP01) to base (AP20). The thicknesses of the lava flows vary between 0.2 and 8 m, with a mode of 2 m (Fig. S1). Basic materials (basalts) have a rapid cooling rate, as compared to acidic lava flows, and in the Apnia sequence, we consider, that they can be estimated to lie within the order of days to weeks, or at most months for the most internal zones. Thus, cooling rates do not seem to vary significantly across the thickness range of studied flows (Fig. S1) and based on field observations we assume that flows are characterized by a similar rate of emplacement. The specimens measured in this study come from drilled cores on the outermost part of each lava flow. The sampled flows were sometimes altered by cracks and micro-faults, and in certain spots were weathered or filled with material from the upper flow, forming veins and pseudo-dikes. Hence, extreme caution was taken during the paleomagnetic sampling, to avoid the altered areas and to look for outcrops of the same lava flows without alteration.

The sequence was sampled with a portable water-cooled drill and the cores were directly oriented in the field with both solar and magnetic compass, and inclinometer. K-Ar ages (±2σ) obtained in these flows yield ages of 3.09 ± 0.10 Ma for flow AP01, 3.28 ± 0.10 Ma for flow AP05, 3.75 ± 0.25 Ma for flow AP07 and 3.70 ± 0.20 Ma for flow AP11 (Lebedev et al., 2008). In a previous paleomagnetic study the Apnia sequence has been described as a polarity transition record (Sánchez-Moreno et al., 2018). The transition recorded would be either Gilbert-Gauss or a composite transition from chron C2Ar to subchron C2An-2n based on its age. However, a record of non-averaged PSV cannot be dismissed, and is not incompatible with the first interpretation.

3. Previous rock magnetic and paleomagnetic results

Rock magnetic experiments performed in a previous paleomagnetic study by Sánchez-Moreno et al. (2018), including IRM acquisition and backfield curves, hysteresis loops and strong field magnetization versus temperature (M_S-T) curves, point to titanomagnetite with varying proportions of titanium and so-called “pseudo-single-domain” (PSD) grain size as the main carrier of the magnetization in the Apnia samples. Samples were grouped by spatial proximity and representative specimens were taken for the rock magnetic experiments to obtain the most representative magnetic characteristics of each flow.

M_S-T curves observed by Sánchez-Moreno et al. (2018) allowed us to distinguish the following behavior types (Figure S2): Type H magnetic samples are characterized by quasi-reversible curves and a single high Curie temperature (T_C) mineral phase near 580°C, corresponding to low-Ti titanomagnetite/magnetite. Type H* samples show a similar behavior as type H samples, with the same low-Ti titanomagnetite phase but initial and final magnetization differed by more than ± 15%. M_S-T curves with successive heatings to peak temperatures of 300°, 400° and 500° show that below these temperatures H* samples are reversible. In some cases, very weak phases with T_C around 615°C appear. This phase might be attributed to the presence of oxidized magnetite (maghemitization). Type L samples display irreversible behavior and two mineral phases. The first phase matches high-Ti titanomagnetite, appearing in the heating curve between 190 °C and 280 °C. The second phase is a high T_C phase observed in both heating and cooling curves, which is interpreted as low-Ti titanomagnetite and represents a tiny fraction of the initial magnetization. Type M samples also show an irreversible behavior and two phases can be distinguished, low-Ti titanomagnetite and an intermediate T_C phase within the 320 °C to 440 °C range, likely high-Ti titanomagnetite. On other hand, the inflection at about 320°C could be titanomaghemite, generated by the oxidation of the titanomagnetite.

Hysteresis parameters (Fig. S3) depicted in a Day plot (Fig. S4) have M_{rs}/M_s values ranging from 0.5 to 0.1, showing what has been referred to as “pseudo-single domain” (PSD) behavior. However, as pointed out by Roberts et al. (2018), Day plots do not allow a simple and direct interpretation of domain states because of the number of variables that influence the hysteresis curve values. Furthermore, Santos and Tauxe (2019) showed that hysteresis parameters have little relationship to reliability of paleointensity results. In the present study, type M and L thermomagnetic curves showed a mixed composition including magnetite, but also titanomagnetite or titanomaghemite with higher Ti content. However, IRM acquisition curves pointed to mainly low coercivity ferrimagnetic phases as carriers of remanence (Sánchez-Moreno et al., 2018), ruling out mixtures of phases with very different coercivities. According to Dunlop (2002), theoretical model curves for single-domain (SD) and multidomain (MD) mixtures match the data for PSD magnetite or titanomagnetites with higher Ti contents (titanomagnetites of composition x =0, 0.2, 0.4 and 0.6), although the SD/MD transition region in grain size is much narrower for titanomagnetite with higher Ti contents than for magnetite without titanium. Thus, the PSD behavior of the studied specimens (Fig. S4) might be explained by a mixture of SD and MD particles although this interpretation is non-unique.

The analysis of paleomagnetic directions and available radiometric data has established that the Apnia sequence records a polarity reversal between 3.75 ± 0.25 Ma and 3.09 ± 0.10 Ma (Sánchez-Moreno et al., 2018). Starting from the base of the section, a succession of 14 reverse polarity lava flows has an average pole that does not match the expected one, which owing to the young age of the sequence is essentially that of a geocentric axial dipole (GAD). The synthetic European apparent polar wander curve (APWP) for the 5 Ma window proposed by Besse and Courtillot (2002) predicts a clockwise deviation of ~17^o in declination and a difference of 2^o in inclination for the location. The expected pole is shown in Fig. 2 and is significantly different from the virtual geomagnetic poles (VGPs) calculated for the lava flows from the present study. A single lava flow above the 14 reverse polarity ones records a “transitional” polarity, with an intermediate VGP latitude of 12.5°. Above this flow, there are five normal polarity flows, which are neither antipodal to the reverse sequence, nor coincident with the expected field direction, and show a counter-clockwise rotation of 27.3°. The possibility of two consecutive rotations in opposite directions in a period between 3.75 and 3.1 Ma seems rather unlikely, hence tectonic rotations are rejected. Directional results do not reflect an EMF behavior as given by a completely stable polarity record and could indicate a polarity transition. According to the radiometric ages, the sequence was interpreted as recording the reverse to normal Gilbert-Gauss reversal or the C2An-2r to C2An-2n one (upper Mammoth transition) within the Gauss chron. A record of a composite transition cannot be rejected, given that a hiatus described by Lebedev et al. (2011a) may coincide in age with the three reversals. The hiatus is located between the phases I (3.75-3.55 Ma) and II (3.30-3.05) of Pliocene volcanism recognized in Djavakheti region. Hence, the reverse lower section would correspond to Chron C2Ar (Gilbert) and the normal upper one to C2An-2n. On the other hand, the mismatch with the pole and the high dispersion could be caused by paleosecular variation (PSV) not being averaged in the record. This second interpretation is supported by the number of directional groups calculated to include the lava flows that show statistically identical paleomagnetic direction: three for the reverse section, one for the transitional lava flow and three for the normal polarity section. Both interpretations, polarity reversal record and non-averaged PSV record are not mutually exclusive (Sanchez-Moreno et al., 2018).

4. Paleointensity methods

In the present study, two different Thellier type methods, Thellier-Thellier (TT) (Thellier and Thellier, 1959) and IZZI (Yu et al., 2004) have been carried out for absolute paleointensity determinations. Thellier type experiments are based on the progressive replacement of the original thermoremanence (TRM) by partial thermal remanences (pTRMs). Consecutive double stepwise heating with and without applied laboratory field (B_{lab}) according to the chosen protocol are performed.

In the Thellier-Thellier (TT) method (Thellier and Thellier, 1959), specimens are heated and cooled twice, in antiparallel laboratory fields, increasing temperatures at each successive pair of steps. The first heating-cooling cycle at a given temperature (T1) is carried out while applying a laboratory field B_{lab} parallel to the z-axis; during the second cycle at T1 the laboratory field B_{lab} is applied in the opposite direction. B_{lab} was set at 40 µT. Lower temperature steps were repeated (the so-called pTRM checks) to assess the occurrence of magnetochemical alterations. An advantage of this method is that both in-field steps are energetically equivalent, which does not happen in other Thellier-type methods in which zero field steps are performed. Thellier-Thellier paleointensity determinations were carried out in the paleomagnetic laboratory of the University of Burgos. Small cylindrical specimens subsampled (8 mm diameter) from oriented standard samples were employed. Heating-cooling in-field routines were carried out under argon atmosphere, specifically aimed at minimizing oxidation of the samples in the TD48-SC (ASC) thermal demagnetizer. Samples were allowed to cool naturally over several hours. The magnetization was measured using a superconducting magnetometer (2G Enterprises). Note that during measurement, in several cases difficulties appeared in exactly preserving specimen orientation. Nevertheless, most specimens could be handled correctly, and accurate measurements were obtained.

The IZZI (Yu et al., 2004) method provides information about so-called pTRM tails attributed to the presence of grains that fail Thellier's Law of reciprocity (Thellier and Thellier, 1959) whereby the unblocking temperature of a component of remanence should be equal to the blocking temperature (a key requirement of paleointensity determinations). The protocol consists of a sequence of alternating double-heating steps: in field and zero field (IZ), heating and cooling at T1, followed by zero field and in field (ZI) at T2, and so on. The laboratory field, B_{lab}, was also set to 40 μT and pTRM checks (Coe, 1967) were also performed. The IZZI method is extremely sensitive to the presence of the pTRM tails, which make the Arai diagrams of specimens whose remanence fails the reciprocity requirement "zig-zag" (Yu et al., 2004; Yu & Tauxe, 2005), allowing detection and elimination of unsuitable specimens. Measurements with the IZZI protocol were carried out in the paleomagnetic laboratory at Scripps Institution of Oceanography, UCSD (USA). In this case, small irregular fragments were taken from standard samples and were prepared in 10 mm diameter vials, previously marked to keep the orientation. The in-house built single chamber thermal demagnetizer and a superconducting magnetometer (2G Enterprise) were used for these measurements.

Pre-selection criteria applied to the chosen samples, for the Thellier-type methods, were the following (i) M_S-T curves should be reasonably reversible (types H and H*), (ii) a single primary paleomagnetic component could be isolated and (iii) at least about 40% of the magnetization still retained at 400°C in demagnetization experiments for the Thellier-Thellier and 60% for the IZZI protocol. Note that the protocols of the two experiments are slightly different in this last point, although not substantially. The criteria are broad, since they are pre-selection, they adapt to the type of samples studied and try to exclude less appropriate cases. As previously mentioned, rock magnetic experiments (Sánchez-Moreno et al., 2018) suggest the presence of titanomagnetites which plot in the region of the Day plot previously interpreted as "PSD" (Figure S4). One of the possible interpretations of this behavior is a mixture of SD and MD grains (Dunlop, 2002), with a significant amount of the samples plotting near MD values, although the mixing curve did not go through any of our data (supplemental information for Sanchez-Moreno et al., 2018). This is interesting as one of the two Thellier-type methods chosen (IZZI) is especially sensitive to the failure of reciprocity, which often is observed in grain populations larger than SD. It should be borne in mind that several other domain state configurations also plot in the PSD area (Roberts et al., 2018) and use of Day plots for domain state interpretation is fraught with difficulty. Moreover, Santos and Tauxe (2019) have shown that while the loose designation of 'PSD' has little predictive value for success in paleointensity experiments, samples with higher ratios of saturation remanence to saturation tend to perform better and those with lower ratios tend to perform worse, there is considerable overlap in behaviors.

Results were considered reliable depending on a set of selection criteria to assess the quality of the experiment conditions, the absence of alteration and the amount of magnetization carried by SD grains. The proposed quality criteria set has been taken from Cromwell et al. (2015a), and two arrays of limit values have been selected to distinguish between two quality levels: The stricter thresholds applied to the selected criteria, are also based on Cromwell et al. (2015a) and are referred to here as CCRIT (Tauxe et al., 2016), while the more relaxed ones, are called here RCRIT. Threshold values of the "relaxed" version are however still stricter than those from other frequently used sets of criteria (e.g. Kissel and Laj, 2004; Leonhardt et al., 2004). The CCRIT and RCRIT criteria and thresholds are the following (to more extensive definitions see Paterson et al. (2014) - Standard Paleointensity Definition):

- $n_{measure} \geq 4$, the number of points on an Arai diagram used to estimate the best-fit linear segment and the paleointensity.
- FRAC ≥ 0.78 and 0.6, NRM fraction used for the best-fit on an Arai diagram determined entirely by vector difference sum calculation (Shaar and Tauxe, 2013).
- $\beta \leq 0.1$, a measure of the relative data scatter around the best-fit line and is the ratio of the standard error of the slope to the absolute value of the slope (Coe et al., 1978).
- SCAT=True, Boolean operator which uses the error on the best-fit Arai plot slope to indicate whether the data over the selected range are too scattered (Shaar and Tauxe, 2013). This statistic provides a test for the scatter of the points on the Arai plot, pTRM checks and pTRM tail checks.
- gmax ≤ 0.6, the maximum gap factor (*g*) between two points determined by vector arithmetic (Shaar and Tauxe, 2013). *g* is a measure of the average NRM lost between successive temperature steps of the segment chosen for the best-fit line on the Arai plot and it reflects the average spacing of the selected points.
- k' ≤ 0.164 and 0.3, the curvature of the Arai plot is determined by the best-fit circle to all of the data (Paterson, 2011), normalized by the respective maximums of the segment NRM and TRM.
- $MAD_{Free} \leq 5°$ and 12º, Maximum Angular Deviation (MAD) of the free-floating, directional fits to the paleomagnetic vector on a vector component diagram (Kirschvink, 1980).
- DANG ≤ 10°, (*Deviation ANGle*) the angle between the free-floating best-fit direction and the direction between data center of mass and the origin of the vector component diagram (Tanaka and Kobayashi, 2003; Tauxe and Staudigel, 2004).
- $n_{pTRM\text{-}check} \geq 2$, the number of pTRM checks used to analyze the best-fit segment on the Arai plot.

At the site level, the CCRIT threshold values require that the number of specimens $n_{SITE,} \geq 3$ and the standard deviation at the site level $\sigma_{site} \leq 4\ \mu T$ and $6\ \mu T$ or $\sigma_{site} \leq 10\%$ and 15% of the mean. The Thellier_GUI (Shaar and Tauxe, 2013) in the PmagPy package software (Tauxe et al., 2016) was used for the interpretation of results obtained with both protocols.

To assess the robustness of our respective criteria CCRIT and RCRIT we evaluate all interpretations for specimens from the Apnia sequence that met these criteria. Then, a bootstrap-like procedure was used, whereby three of the interpretations per site were selected at random and their mean was calculated. If the resulting "site mean" passed the site level criteria for standard deviation, these were included in the "accepted site means". This procedure was repeated 1000 times. The simulated results were compared with the expected field at each site. They are plotted in Fig. 3a as red circles or white squares for the RCRIT and CCRIT criteria respectively. The R^2 value (coefficient of determination of the linear regression) of the RCRIT was 0.92, while that for CCRIT was 0.94. It is likely that for the strongest field, the results suffer a non-linear TRM acquisition and the ancient field was underestimated.

The differences between the calculated and expected fields for the 1000 simulated site means are plotted in Fig. 3b. The median difference for RCRIT was -2 μT, while that for CCRIT was less than 1 μT and the range of differences for RCRIT was -14.8 to +15.5 μT while that for CCRIT was -12.9 to 9.0 μT. It is therefore evident that while the stricter criteria do outperform the more relaxed version, the penalty is not very large.

5. Results

In order to obtain a full image of the paleointensity record, the measurements with the different methods have been carried out trying to include the maximum number of lava flows of the sequence. However, the number of analyzed samples was, limited by pre-selection criteria, i.e., mineralogical characteristics and thermal behavior of the analyzed samples.

A total of 55 mini-samples were subjected to the original paleointensity determination protocol proposed by Thellier and Thellier (1959). The samples were taken from all lava flows of the sequence. In most cases three determinations per flow were performed, except for those in which thermomagnetic curves of some specimens yielded two mineral phases (M and L type), in which case fewer could be carried out. None of the TT experiments passed the strict CCRIT thresholds (Table 1). The somewhat relaxed RCRIT threshold values allowing slightly more scattered directions and somewhat more curved results with a slightly lower fraction of remanence yielded four acceptable TT interpretations from lava flows AP04, AP14 and AP18 (Table 1.). Problems in keeping some specimen orientations during TT experiments occurred (see Fig. 4d). This resulted in MAD and DANG values in excess of even the relaxed thresholds RCRIT for acceptance. These results, together with the curved Arai plots, finally have only allowed four TT determinations that could be taken for the flow-averages. Examples of representative experiments are shown in Figures 4a, b, c and d. Interestingly, the primary reason for failure of the Thellier-Thellier (TT) experiments for lava flows with successful IZZI experiments (see below) was curvature (the k' criterion of Paterson et al., 2014), due to poorer laboratory handling. Santos and Tauxe (2019) showed that curvature greater than 0.164 was associated with lower precision of paleointensity estimates, which if too few specimens were analyzed could lead to less accurate results.

A total of 100 specimens from all 20 flows that constitute the Apnia sequence were chosen for paleointensity experiments with the IZZI method (Yu et al., 2004). A minimum of two determinations per flow were performed, in some cases even from the same core, and depending on the sample availability, up to eight. Results of representative experiments are shown in Figure 4. A total of six specimens from three lava flows (AP04, AP14 and AP18) passed the CCRIT thresholds. As the CCRIT criteria also require at least three specimens from each lava flow to pass and to agree with one another within some tolerance, none of the experiments conducted here pass the strict CCRIT criteria. Using the looser RCRIT criteria, 41 specimens from ten lava flows (AP01, AP04, AP07, AP11, AP14, AP16, AP17, AP18, AP19 and AP20) (Table 1) yield acceptable paleointensity determinations.

There is no significant theoretical difference between the classical Thellier-Thellier and the IZZI methods. Under ideal conditions, both should yield identical answers and if the data are treated in a consistent manner, they can be combined at the site level and analyzed jointly. Therefore, we combined the two data sets and ran the Thellier GUI auto interpreter (Shaar and Tauxe, 2013) optimizing the standard deviation at the site level to choose from the acceptable interpretations. The only exception was flow AP16, in which, as will be explained below, results were interpreted manually. With this procedure, a total of eight sites passed RCRIT criteria, with a maximum standard deviation at the site level of 4.3 μT and three to eight acceptable specimens per flow (see Table 2).

6. Discussion

6.1. Data analysis

The analysis of paleointensity data can be very sensitive to interpretation, and for this reason, a strict set of quality criteria has been applied automatically. However, there are cases in which it is necessary to perform an analysis "by hand" of the possible results, as long as it is based on rigorous and objective criteria. In the analysis of Apnia sequence data we have found some examples in which it is necessary to examine the results by lava flow visually. This was the case of flow AP16. As mentioned in Section 5, the average for the AP16 flow has been calculated manually. This flow yields seven determinations that meet the relaxed selection criteria, but two of them show suspicious two-slope Arai plots and the paleointensity obtained is significantly greater than in other flows of the sequence. Therefore, these two determinations have been rejected by the automated analysis. For the remaining determinations of the flow, the interval of 350 to 600°C has been taken to optimize the adjustment to the requirements per site. Another special case is the flow AP17. The mean paleointensity obtained shows a standard deviation of 4.3 µT, which corresponds to 18.9%. This high percentage is due to two differentiated groups of three specimens each, the first one around 27 µT and the second one around 18 µT. We have decided to take the average of all six determinations because they are all of high quality and the result obtained is consistent with the results in whole sequence. Note also that AP04 displays one lower paleointensity value of 26.6 µT, which technically is included, but without it, the flow average would be increased. Two flows, AP01 and AP07 yield valid data, but do not meet the minimum of three determinations per site, so that they had to be excluded.

Finally, eight mean flow paleointensity values have been obtained from this work. In the present study, application of the usual criteria (e.g. Kissel and Laj, 2004; Leonhardt et al., 2004), would yield a greater number of apparently reliable results. However, this work is focused on obtaining data of high reliability and quality. Given their trustworthiness and robustness, the paleointensities obtained under the proposed especially strict quality criteria should be especially useful for the development of EMF models.

There are additional factors that could cause significant bias to site averaged paleointensity results (sites are different lava flows, in our case). Biggin and Paterson (2014) and Kulakov et al. (2019) propose a new set of qualitative criteria (Q_{PI}) to assess the data reliability. They identify several biasing agents applicable to paleointensity measurements which sometimes are not taken in account in studies. In the following lines we discuss to which extent our results from the Apnia sequence match with the Q_{PI} criteria.

- AGE: Assesses whether the associated absolute age estimate, remanence component structure, and paleomagnetic direction are consistent with a reliable and useful paleointensity. Apnia paleointensity results are linked to reliable K-Ar age and paleomagnetic behaviour derived from a primary component of remanence (Sánchez-Moreno et al., 2018).

- STAT: Sufficient number of specimens to test whether the paleointensity result consistency is reasonable to have a moderate precision ($n_{specimen} \geq 5$). Six lava flows passed the requirement of at least five individual specimens used for the paleointensity average (AP04, 14, 16, 17, 18 and 19). Two flows have a 3-

specimens average (AP11 and 20), which commonly, is still considered a good average.

- TRM: The remanence must be thermal so that the paleointensity acquisition performed in the laboratory is proportional to that produced by the EMF at the time of rock magnetization. Rock magnetic results point to remanence being a TRM in samples used for paleointensity determinations. The fact that these are lava flows involves a TRM because the volcanic rocks undergo a cooling at the moment of their formation, although we do not have independent petrological evidence.

- ALT: Heating induced alteration is a major threat to the accuracy of paleointensity measurements. pTRM checks and rock-magnetism experiments (thermomagnetic curves) support that there is not alteration in Apnia specimens.

- MD: Reasonable evidence that the final estimate was not significantly biased by multidomain behavior during the experiment. High FRAC parameter (≤ 0.6) verify that the MD effect does not affect the final paleointensity estimate.

- ACN:

1. Cooling rate: The characteristics of the studied lava flows (thickness, composition, etc., see section 2) allow the assumption that the cooling-rate does not affect the paleointensity experiments, given that it does not vary significantly in the range of thickness of the individual cooling units, although (Santos and Tauxe, 2019) have shown that cooling rate dependence is difficult to predict. As far as the cooling-rate dependence is concerned, the Thellier-Thellier and IZZI experiments have been performed by leaving the samples cool down naturally (~10h) and with a fan (~1h) respectively, without differences in the results.

2. Anisotropy of TRM: In order to analyze the influence of the anisotropy of remanence on our results, we have used the anisotropy of magnetic susceptibility (AMS) as a proxy. We measured AMS on one sample from each flow, at the beginning of the paleomagnetic study of the Apnia sequence, and in all cases a very low anisotropy was observed, with a corrected anisotropy P' value (Jelinek, 1981) of approximately 4% (P' between 1 and 1.040, average 1.014). In addition, we calculated the gamma statistic γ (Paterson et al., 2014; Standard Paleointensity Definitions, SPD), which detects in many cases the influence of anisotropic TRM (in the case where the lab field is applied along one of the eigenvectors. The requirement of multiple unoriented specimens guards against this unlikely scenario). Both the Thellier-Thellier and IZZI

determinations, yielded values between 0.2° and 3.7°. These results suggest that anisotropy of remanence does not play an important role in our samples, as only when gamma >> 4° it is considered that there is a higher chance that the specimen is anisotropic (Paterson et al., 2015).

3. Non-linear TRM effects: The non-linear dependence of TRM on applied field is minimal when the laboratory and ancient field strengths are approximately equal (Paterson, 2013; Selkin et al., 2007). For most typical geological materials (i.e., lavas) if both fields are within ∼1.5 times each other, then the influence of non-linear TRM is likely to be minimal (Biggin and Paterson, 2014a).

- TECH: Estimate is an average of results from more than one paleointensity technique. In Apnia sequence, final paleointensity on three lava flows has been calculated from more than one Thellier-type technique (AP04, 14 and 18), nevertheless Thellier-Thellier and IZZI methods are non-independent, so these paleointensity averages do not meet the criterion.

- LITH: Estimate is an average of results from more than one lithology or from samples from the same lithology showing significantly different unblocking behavior. The paleointensity estimations in Apnia have been performed over samples of similar lithology and with similar unblocking behaviour.

As a result, six lava flows (AP04, AP14, AP16, AP17, AP18 and AP19) yield Q_{PI} = 5 and in only two cases (AP11 and AP20) Q_{PI} = 4. According to Biggin and Paterson (2014), 60% of the paleointensity values collected in the PINT database (updates between 2012.08 and 2014.01) show a Q_{PI} score of 1, 2 and 3. The data obtained in the Apnia sequence show a higher quality than the mean, according to the Q_{PI} evaluation methodology.

6.2. Directional results vs. paleointensities

Paleomagnetic directions of the Apnia sequence might show a (perhaps partial) polarity reversal, or a composite reversal (Sánchez-Moreno et al., 2018). According to radiometric ages (Lebedev et al., 2008), the sequence could record the reverse to normal C2Ar to C2An-3n (Gilbert-Gauss) polarity change or its reverse lower part could correspond to chron C2Ar and the upper part to C2An-2n. The Apnia sequence is composed of two subsections recording different polarities, which are not antipodal, separated by a single flow with a transitional direction (Fig. 2). Based on the analysis of paleomagnetic directions, virtual geomagnetic poles scatter, directional groups and a few previously available paleointensity results (Calvo-Rathert et al., 2013), two differing though not conflicting interpretations were proposed for the sequence (Sánchez-

Moreno et al., 2018): 1) An anomalous EMF record and 2) a short recording time unable to average paleosecular variation.

1) Anomalous EMF record (reflecting a polarity reversal or composite reversal)

In the present study, paleointensity values between 16.8 and 26.8 µT in the lower reverse polarity section have been obtained, while a single determination in the upper normal-polarity section yields a higher single value of 32.1 µT. At present, the EMF intensity in Georgia is 49 µT under a presumably stable magnetic field regime, significantly higher than the values obtained for the Apnia lavas. This disagreement could be due to the Apnia lavas being emplaced during a polarity transition as there is a general accord among the paleomagnetic community that during large deviations of the geomagnetic field from the axial dipole position the intensity decreases (e.g. Valet et al., 2005). Another observed characteristic of polarity transitions is that their onset is often first found in the intensity record and later in the directional one (e.g. Herrero-Bervera and Valet, 1999; Prévot et al., 1985), similarly to the observed low field values in the Apnia lavas before the transitional direction. Considering these references, it is possible to interpret that the lower part of the Apnia sequence records the intensity drop, starting to the reversal, whereas the upper section shows the recovery of the EMF intensity, after the reversal.

Nevertheless, an isolated record of a stable EMF would also be a possible interpretation of the lower section of Apnia sequence if we consider it as independent from transitional and subsequent normal polarity upper section. Besides the lower section show VGPs closer to the expected pole than the upper one (Fig. S2). In fact, the angular dispersion analysis over lower Apnia VGPs with respect to the expected pole, shows values within the range proposed by the PSV models in lavas (Sánchez-Moreno et al., 2018).

2) Short recording time unable to average paleosecular variation (PSV)

On the other hand, assuming that a limited number of directional groups was determined over the 20 flows of Apnia sequence (three of reverse polarity, one transitional and three of normal polarity), a short time of emplacement for the different flow groups is suggested. It is therefore possible that this low amount of independent data represents snapshots of the field and does not average out secular variation.

We have to be mindful that the term PSV describes temporal variations in the field, meaning not only variations of declination and inclination, but also in intensity. As in directional studies, a non-averaged PSV also indicates that the virtual axial dipole moment (VADM), obtained from the intensity at a specific location, represents a spot image of the EMF variation and cannot be taken as a GAD value for that time. Likewise, the virtual geomagnetic pole (VGP), corresponding to the EMF direction obtained for the same data, would not represent the GAD. This can lead to confusion with a transitional record, where the GAD is very weak and therefore the VGP does not coincide with the geographic north and the VADM value is anomalous.

Now, the question to be posed is how long the averaged period should be to make sure that a representative value of the time-averaged field is obtained. Traditional analysis of long-term PSV covers periods longer than10^5-10^6 years (e.g. Harrison, 2007; Johnson et al., 2008; Johnson and Constable, 1996; McElhinny et al., 1996; Merrill et al., 1996). However, there are also studies on datasets that cover a smaller timescale. Barton (1982) used sediment records to suggest that timescales of at least 10^3 years provided reasonable estimates of PSV, as well as studies that suggest at least 10^4–10^5 years (Carlut et al., 1999; Merrill and McFadden, 2003), while Lund (2018) considers a scale of 10^3-10^5. Constable and Johnson (2005) perform a power spectrum analyses from 10^7 to 10^2 years where the spectrum between 10^1 to 10^4 years is taken to characterize the PSV. Our sequence is in the range of 10^5 years, which is likely to support a record where the PSV is averaged.

On the other hand, the paleointensity values obtained in Apnia might also reflect a weak time-averaged field (TAF) during a stable regime. The observed low field strength is not inconsistent with other paleointensity records for this time period (e.g. Cromwell et al., 2015b; Juarez and Tauxe, 2000, Wang et al., 2015).These are TAF results obtained with high quality paleointensity data and analysis of the global database (MAGIC) excluding non-ideal data (Juárez et al., 1998; Tauxe et al., 2013).

6.3. Global VADMs during the 3-4 Ma

Flow-average paleointensities obtained range from 16.8 μT to 32.1 μT. Translating intensity values to virtual axial dipole moments (VADM), yields values between 28.6 and 54.6 ZAm^2. The mean for the whole sequence is 38.9 ZAm^2, which is half of the present VADM (~80 ZAm^2).

Analysis of paleointensity results of stable polarity periods during the last 5 My have come to different conclusions. There are studies suggesting VADM averages of 55 ZAm^2 (Juárez and Tauxe, 2000) and 36 ZAm^2 (Yamamoto and Tsunakawa, 2005) and (Cromwell et al., 2015b) obtained values of 47 ZAm^2 for the last 5 My, a similar value as that suggested by Tauxe et al. (2004a) for the Brunhes-Matuyama transition (49 ZAm^2). On the other hand, older studies based on less restrictive selection criteria resulted in VADM values close to the present one (Goguitchaichvili et al., 1999; Heller et al., 2002; McFadden and McElhinny, 1982; Smirnov and Tarduno, 2003). For older and longer periods VADM averages of 42-48 ZAm^2 for the 0-160 My range (Juárez et al., 1998; Tauxe, 2006; Tauxe et al., 2013) have been suggested while the older study of Tanaka et al. (1995) estimated the average dipole moment for the last 20 Ma to be approximately 84 ZAm^2. It should be noted that significantly lower values are found in the Mesozoic, during the so-called Mesozoic dipole low (Biggin and Thomas, 2003; Perrin and Shcherbakov, 1997; Prévot et al., 1990), which might reduce the average value in calculations including the last 160 or 300 My. Due to the high temporal and spatial variability of the EMF, some caution should be however applied when comparing the results from the short Apnia sequence, which records a period of less than 1 My at 40° latitude, with the results from different intervals of the global databases (i.e. PINT and MagIC). If we separate the values obtained in the normal (upper) and reverse (lower) sequences, considering they are not antipodal and do not match the GAD, we obtain 54.6 and 36.6 ZAm^2 respectively. Therefore, the VADM average of the lower Apnia, prior to the polarity change, is below the most recent estimates of the VADM median value calculated for the last 5 My, but comparable to those suggested by Lawrence et al. (2009) and Cromwell et al. (2015b) from high latitude sites.

The results have also been compared with VADMs obtained in different locations for the 3 - 4 Ma age interval, which is the period covered by the Apnia sequence (PINT 2015.05, Biggin et al., 2010) (Table S1 and Fig. 6.). The data have been filtered allowing only paleointensities from Thellier-type methods with pTRM checks. Nonetheless, the selection criteria applied to this data are those commonly used (Leonhardt et al., 2004). The results from the Djavakheti Highland have been compared separately and show both higher and equivalent VADM values with respect to the present study (Table S1 and Fig. 6.b). Calvo-Rathert et al. (2011) obtain an average VADM of 66 ZAm^2 on different sequences from the Djavakheti Highland. Calvo-Rathert et al. (2013) obtain results on some samples from the Apnia sequence, ranging between 29 and 130 ZAm^2. This last work was performed on specimens sub-sampled from blocks taken in samplings in 1984-1986, in which besides a possible orientation error, no information about the specific stratigraphic order of each lava flow was available. Then, we have used paleomagnetic information from Calvo-Rathert et al. (2013) to try to correlate their results and those of the present study (Table S3). Four paleointensity results have been correlated with the lower section of inverse polarity, thanks to the directional groups obtained in Sanchez-Moreno et al. (2018). Values of 76.1 µT (n=1) and 17.3 µT (n=5) match the three lowest flows. The second one is clearly in better agreement with the values obtained in the present study and having been obtained from an average of 5 determinations also can be considered more reliable. Matching with our AP11 flow, Calvo-Rather et al. (2013) obtains a similar value of 27.4 µT (n=2). In the upper normal polarity section we found a coincidence with the directions obtained in flow AP04, but the result obtained by Calvo-Rathert et al. (2013) displayed a much higher paleointensity value (54.3 µT, n=2). Although in the present study we could not obtain results for the transitional polarity flow , Calvo-Rathert et al. (2013) obtained a paleointensity result of 26 μT (n=1) in Masa flow characterized by a transitional VGP. Thus, only some coincidences can be observed with the study of Calvo-Rathert et al. (2013). In other studies performed in the Djavakheti highland, Goguitchaichvili et al., (2009) yield the lowest values ranging from 12 to 55 ZAm^2, while Camps et al. (1996) obtain, mostly paleointensities within the range obtained in this work (Table S1 and Fig. 6.b). The low intensities observed by Goguitchaichvili et al. (2009) and Camps et al. (1996) are related to the Gilbert-Gauss reversal, as could be the data from the present study.

Regarding locations outside Georgia, 112 VADM data points within the age range of 3 to 4 Ma have been extracted from the PINT15.05 database (Biggin et al., 2010) taking only data from Thellier-type methods with pTRM checks. These data, show a very scattered distribution (Table S1 and Fig. 6.a). Therefore, it is not possible to observe any correlation with the dataset obtained in the present work. This analysis brings to light the problem of the global paleointensity database which needs to be completed with a more uniform distribution around the globe and uniformity in the quality of the data.

For comparison, we downloaded the paleointensity measurements available in the MagIC database (www2.earthref.org/MagIC/search) for the age range 2.5-4.5 Ma (Lawrence et al., 2009; Tauxe, 2006; Tauxe et al., 2004; Tauxe and Staudigel, 2004) and reinterpreted them applying the selection criteria set RCRIT, employed in the current study (Table S2). The number of results, as expected, is far fewer under these stricter criteria than in the original studies (in particular, none of the determinations performed in Calvo-Rathert et al. (2013) passes the RCRIT criteria.). The VADMs that pass our criteria have an average of 48.6 ZAm^2, higher than those obtained in the lower section of the Apnia sequence (36.6 ZAm^2), prior to the polarity change. This would be in agreement with the intensity drop observed at pre-transitional moments, although an isolated record of a stable EMF cannot be discarded for the lower part of Apnia section. This interpretation would support a weak time-averaged field, although the effect of non-averaged PSV should also be taken into account. The latter could also apply to the high intensity observed in the upper Apnia section.

7. Conclusions

An absolute paleointensity determination study has been carried out on the Pliocene Apnia sequence composed of 20 lava flows. Directional paleomagnetic results obtained by Sánchez-Moreno et al. (2018) on this sequence provide two different though not conflicting interpretations, a short recording time unable to average PSV and/or an anomalous EMF record. The lower reverse polarity Apnia section seems to average the PSV, while the upper normal polarity section shows a wider scatter. According to available radiometric ages, the sequence might record the Gilbert-Gauss transition, although a composite transition record from chron C2Ar to subchron C2An-2n cannot be discarded (Sánchez-Moreno et al., 2018).

A total of 55 paleointensity determinations were carried out using the Thellier-Thellier method and 100 with the IZZI method. We obtained four successful Thellier-Thellier determinations and 41 IZZI determinations, under the proposed RCRIT thresholds, although none met the stricter CCRIT set. The still very stringent RCRIT set thus allowed a selection of 45 high quality and reliable paleointensity determinations.

Application of the RCRIT criteria at site level yields average paleointensity results in eight of the 20 studied lava flows. VADM values between 28.6 and 45.6 ZAm^2 have been obtained in the lower reverse section. The (single) normal polarity determination from the upper section shows, however, a higher value of 54.6 ZAm^2. These values are well below the present-day dipole moment in Georgia (84 ZAm^2) and the mean VADM obtained by Tanaka et al. (1995) for the last 20 My. On the other hand, more recent studies using stricter criteria have obtained VADM averages for the last 5 Ma between 36 and 55 ZAm^2 (Juarez and Tauxe, 2000; Yamamoto and Tsunakawa, 2005) in agreement with those obtained in the present study in the Apnia sequence.

The relatively low paleointensity values obtained on the flows erupted before the lava flow that recorded a transitional polarity support the hypothesis that the reverse polarity section of the Apnia sequence recorded a transitional EMF intensity. These results suggest that the paleointensity drops before the complete directional reversal. The higher value obtained after the reversal depicts the recovery of the EMF intensity, still within an anomalous regime. The data obtained are consistent with the observation that the intensity decreases significantly during polarity reversals (Valet et al., 2005) and that this decrease is observed before the onset of directional anomalies (e.g. Prévot et al., 1985). The paleointensity recorded in the normal polarity upper section are slightly higher, probably showing a trend towards a more stable field regime. However, the paleointensity results obtained in lower Apnia yield data for only seven flows from three directional groups. Thus, an isolated record of a stable EMF cannot be discarded. This interpretation would support a weak time-averaged field, although the effect of non-averaged PSV cannot be excluded.

Acknowledgements

This work was supported by project CGL2012-32149 (Ministerio de Economía y Competitividad, Spain), project BU066U16 (Junta de Castilla y León, Spain), pre-doctoral grant BES-2013-064060 (Ministerio de Economía y Competitividad, Spain) and by National Science Foundation (USA) grant EAR1345003. AG is grateful to financial support given by DGAPA-PAPIIT IN101717. MCR acknowledges funding from the Fulbright Commission and the Spanish Ministry of Science, Innovation and Universities for a research stay at Hawaii University at Manoa. The data used in this work are listed in the tables and references and can be found in the MagIC online data repository at https://earthref.org/MagIC. Reviewers are acknowledged for their constructive comments and suggestions, which have helped to improve this manuscript.

References

Adamia, S., Zakariadze, G., Chkhotua, T., Sadradze, N., Tsereteli, N., Chabukiani, A., Gventsadze, A., 2011. Geology of the Caucasus: A Review. Turkish J. Earth Sci. 20, 489–544. doi:10.3906/yer-1005-11

Avagyan, A., Sosson, M., Karakhanian, A., Philip, H., Rebai, S., Rolland, Y., Melkonyan, R., Davtyan, V., 2010. Recent tectonic stress evolution in the Lesser Caucasus and adjacent regions. Geol. Soc. London, Spec. Publ. 340, 393–408. doi:10.1144/sp340.17

Barton, C.E., 1982. Spectral Analysis of Palaeomagnetic Time Series and the Geomagnetic Spectrum. Philos. Trans. R. Soc. A Math. Phys. Eng. Sci. 306, 203–209. doi:10.1098/rsta.1982.0080

Besse, J., Courtillot, V., 2002. Apparent and true polar wander and the geometry of the geomagnetic field over the last 200 Myr. J. Geophys. Res. 107, 2300. doi:10.1029/2000JB000050

Biggin, A.J., McCormack, A., Roberts, A., 2010. Paleointensity Database Updated and Upgraded. Eos, Trans. Am. Geophys. Union 91, 15. doi:10.1029/2010EO020003

Biggin, A.J., Paterson, G. a., 2014a. A new set of qualitative reliability criteria to aid inferences on palaeomagnetic dipole moment variations through geological time. Front. Earth Sci. 2, 1–9. doi:10.3389/feart.2014.00024

Biggin, A.J., Paterson, G.A., 2014b. A new set of qualitative reliability criteria to aid inferences on palaeomagnetic dipole moment variations through geological time. Front. Earth Sci. 2, 1–9. doi:10.3389/feart.2014.00024

Biggin, A.J., Perrin, M., Dekkers, M.J., 2007. A reliable absolute palaeointensity determination obtained from a non-ideal recorder 257, 545–563. doi:10.1016/j.epsl.2007.03.017

Biggin, A.J., Thomas, D.N., 2003. Analysis of long-term variations in the geomagnetic poloidal field intensity and evaluation of their relationship with global geodynamics. Geophys. J. Int. 152, 392–415. doi:10.1046/j.1365-246X.2003.01849.x

Calvo-Rathert, M., Bógalo, M.F., Gogichaishvili, A., Sologashvili, J., Vashakidze, G., 2013. New paleomagnetic and paleointensity data from Pliocene lava flows from the Lesser Caucasus. J. Asian Earth Sci. 73, 347–361. doi:10.1016/j.jseaes.2013.04.039

Calvo-Rathert, M., Gogichaishvili, A., Vashakide, G., Sologashvili, J., 2015. New paleomagnetic and paleointensity data from Georgia (Caucasus): a review. Latinmag Lett. 5, 1–23.

Calvo-Rathert, M., Goguitchaichvili, A., Bógalo, M.F., Vegas-Tubía, N., Carrancho, Á., Sologashvili, J., 2011. A paleomagnetic and paleointensity study on Pleistocene and Pliocene basaltic flows from the Djavakheti Highland (Southern Georgia, Caucasus).

Phys. Earth Planet. Inter. 187, 212–224. doi:10.1016/j.pepi.2011.03.008

Calvo-Rathert, M., Morales-Contreras, J., Carrancho, Á., Goguitchaichvili, A., 2016. A comparison of Thellier-type and multispecimen paleointensity determinations on Pleistocene and historical lava flows from Lanzarote (Canary Islands, Spain). Geochemistry, Geophys. Geosystems 17, 3638–3654. doi:10.1002/2016GC006396

Camps, P., Ruffet, G., Shcherbakov, V.P., Shcherbakova, V. V., Prévot, M., Moussine-Pouchkine, A., Sholpo, L., Goguitchaichvili, A., Asanidzé, B., 1996. Paleomagnetic and geochronological study of a geomagnetic field reversal or excursion recorded in pliocene volcanic rocks from Georgia (Lesser Caucasus). Phys. Earth Planet. Inter. 96, 41–59. doi:10.1016/0031-9201(95)03110-3

Carlut, J., Courtillot, V., Hulot, G., 1999. Over how much time should the geomagnetic field be averaged to obtain the mean-palaeomagnetic field ? Terra Nov. 11, 239–243. doi:10.1046/j.1365-3121.1999.00253.x

Coe, R.S., 1967. Paleo-intensities of the Earth’s magnetic field determined from Tertiary and Quaternary rocks. J. Geophys. Res. 72, 3247–3262. doi:10.1029/JZ072i012p03247

Coe, R.S., Grommé, S., Mankinen, E.A., 1978. Geomagnetic paleointensities from radiocarbon-dated lava flows on Hawaii and the question of the Pacific nondipole low. J. Geophys. Res. Solid Earth 83, 1740–1756. doi:10.1029/JB083iB04p01740

Constable, C., Johnson, C., 2005. A paleomagnetic power spectrum. Phys. Earth Planet. Inter. 153, 61–73. doi:10.1016/j.pepi.2005.03.015

Cromwell, G., Tauxe, L., Halldórsson, S.A., 2015a. New paleointensity results from rapidly cooled Icelandic lavas: Implications for Arctic geomagnetic field strength. J. Geophys. Res. Solid Earth 120. doi:10.1002/2014JB011828

Cromwell, G., Tauxe, L., Halldórsson, S.A., 2015b. New paleointensity results from rapidly cooled Icelandic lavas : Implications for Arctic geomagnetic field strength. J. Geophys. Res. Solid Earth 120. doi:10.1002/2014JB011828

Cromwell, G., Tauxe, L., Halldõrsson, S.A., 2015c. New paleointensity results from rapidly cooled Icelandic lavas: Implications for Arctic geomagnetic field strength. J. Geophys. Res. Solid Earth 120. doi:10.1002/2014JB011828

Cromwell, G., Tauxe, L., Staudigel, H., Ron, H., 2015d. Paleointensity estimates from historic and modern Hawaiian lava flows using glassy basalt as a primary source material. Phys. Earth Planet. Inter. 241, 44–56. doi:10.1016/j.pepi.2014.12.007

Doubrovine, P. V., Veikkolainen, T., Pesonen, L.J., Piispa, E., Ots, S., Smirnov, A. V., Kulakov, E. V., Biggin, A.J., 2019. Latitude Dependence of Geomagnetic Paleosecular Variation and its Relation to the Frequency of Magnetic Reversals: Observations From the Cretaceous and Jurassic. Geochemistry, Geophys. Geosystems 20, 1240–1279. doi:10.1029/2018GC007863

Dunlop, D.J., 2002. Theory and application of the Day plot (Mrs/Ms versus Hcr/Hc) 1. Theoretical curves and tests using titanomagnetite data. J. Geophys. Res. 107, EPM4-1-EPM4-22. doi:10.1029/2001JB000486

Glatzmaier, G.A., Coe, R.S., 2015. Magnetic Polarity Reversals in the Core, in: Schubert, G. (Ed.), Treatise on Geophysics. Elsevier, pp. 279–295. doi:10.1016/B978-0-444-53802-4.00146-9

Goguitchaichvili, A., Calvo-Rathert, M., Sologashvili, J., Morales, J., Soler, A.M., Espinosa, M., 2001. A reconnaissance magnetostratigraphy of Georgian Plio-Quaternary volcanic provinces (southern Caucasus). Geofis. Int. 40, 111–119.

Goguitchaichvili, A., Calvo, M., Sologashvili, D., Alva, L., Urrutia, J., Calvo-Rathert, M., Sologashvili, D., Alva, L., Urrutia, J., 2000. Palaeomagnetism of Georgian Plio-Quaternary volcanic provinces (Southern Caucasus): a pilot study. Comptes Rendus l'Académie des Sci. - Ser. IIA - Earth Planet. Sci. 331, 683–690. doi:10.1016/S1251-8050(00)01471-3

Goguitchaichvili, A., Cervantes, M.A., Calvo-Rathert, M., Camps, P., Sologashvili, J., Maissuradze, G., 2009. Gilbert-Gauss geomagnetic reversal recorded in Pliocene volcanic sequences from Georgia (Lesser Caucasus): revisited. Earth, Planets Sp. 61, 71–81. doi:10.1186/BF03352886

Goguitchaichvili, A.T., Prévot, M., Camps, P., 1999. No evidence for strong fields during the R3-N3 Icelandic geomagnetic reversal. Earth Planet. Sci. Lett. 167, 15–34. doi:10.1016/S0012-821X(99)00010-2

Harrison, C., 2007. Secular variation model, in: Gubbins, D., Herror-Bervera, E. (Eds.), Encyclopedia of Geomagnetism and Paleomagnetism. Springer Publishing, pp. 892–901.

Heller, R., Merrill, R.T., McFadden, P.L., 2002. The variation of intensity of earth's magnetic field with time. Phys. Earth Planet. Inter. 131, 237–249. doi:10.1016/S0031-9201(02)00038-9

Herrero-Bervera, E., Valet, J.-P.P., 1999. Paleosecular variation during sequential geomagnetic reversals from Hawaii. Earth Planet. Sci. Lett. 171, 139–148. doi:10.1016/S0012-821X(99)00145-4

Hill, M.J., Shaw, J., Herrero-Bervera, E., 2005. Palaeointensity record through the Lower Mammoth reversal from the Waianae volcano, Hawaii. Earth Planet. Sci. Lett. 230, 255–272. doi:10.1016/j.epsl.2004.11.012

Jelinek, V., 1981. Characterization of the magnetic fabric of rocks. Tectonophysics 79, T63–T67. doi:10.1016/0040-1951(81)90110-4

Johnson, C.L., Constable, C.G., 1996. Palaeosecular variation recorded by lava flows over the past five million years. Phil. Trans. R'. Soc. Lond. A 354, 89–141. doi:10.1098/rsta.1996.0004

Johnson, C.L., Constable, C.G., Tauxe, L., Barendregt, R., Brown, L.L., Coe, R.S., Layer, P., Mejia, V., Opdyke, N.D., Singer, B.S., Staudigel, H., Stone, D.B., 2008. Recent investigations of the 0-5 Ma geomagnetic field recorded by lava flows. Geochemistry, Geophys. Geosystems 9, n/a-n/a. doi:10.1029/2007GC001696

Johnson, C.L., Constable, C.G., Tauxe, L., Barendregt, R., Brown, L.L., Coe, R.S., Layer, P., Mejia, V., Opdyke, N.D., Singer, B.S., Staudigel, H., Stone, D.B., 2008. Recent investigations of the 0–5 Ma geomagnetic field recorded by lava flows. doi:10.1029/2007GC001696

Juarez, M.T., Tauxe, L., 2000. The intensity of the time-averaged geomagnetic field: the last 5 Myr. Earth Planet. Sci. Lett. 175, 169–180. doi:10.1016/S0012-821X(99)00306-4

Juárez, M.T., Tauxe, L., Gee, J.S., Pick, T., 1998. The intensity of the Earth's magnetic field over the past 160 million years. Nature 394, 878–881. doi:10.1038/29746

Kirschvink, J.L., 1980. The least-squares line and plane and the analysis of palaeomagnetic data. Geophys. J. R. Astron. Soc. 62, 699–718. doi:10.1111/j.1365-246X.1980.tb02601.x

Kissel, C., Laj, C., 2004. Improvements in procedure and paleointensity selection criteria (PICRIT-03) for Thellier and Thellier determinations: Application to Hawaiian basaltic long cores. Phys. Earth Planet. Inter. 147, 155–169. doi:10.1016/j.pepi.2004.06.010

Kulakov, E.V., Sprain, C., Doubrovine, P.V., Smirnov, A.V., Paterson, G.A., Hawkins, L., Fairchild, L., Piispa, E.J., Biggin, A.J., 2019. Analysis of an updated paleointensity database (Q PI -PINT) for 65-200 Ma: Implications for the long-term history of dipole moment through the Mesozoic. J. Geophys. Res. Solid Earth 2018JB017287. doi:10.1029/2018JB017287

Lawrence, K.P., Tauxe, L., Staudigel, H., Constable, C.G., Koppers, A., McIntosh, W., Johnson, C.L., 2009. Paleomagnetic field properties at high southern latitude. Geochemistry, Geophys. Geosystems 10. doi:10.1029/2008GC002072

Lebedev, V.A., 2015. Geological map of Javakheti volcanic area (Lesser Caucasus), 1/200000, (2015). doi:10.13140/RG.2.1. 610 2359.2169

Lebedev, V.A., Bubnov, S.N., Dudauri, O.Z., Vashakidze, G.T., 2008. Geochronology of Pliocene volcanism in the Dzhavakheti Highland (the Lesser Caucasus). Part 1: Western part of the Dzhavakheti Highland. Stratigr. Geol. Correl. 16, 204–224. doi:10.1134/S0869593808020081

Lebedev, V.A., Chernyshev, I. V., Sharkov, E. V., 2011. Geochronological scale and evolution of late Cenozoic magmatism within the Caucasian segment of the alpine belt. Dokl. Earth Sci. 441, 1656–1660. doi:10.1134/S1028334X11120051

Leonhardt, R., Heunemann, C., Krasa, D., 2004. Analyzing absolute paleointensity determinations: Acceptance criteria and the software ThellierTool4.0. Geochemistry, Geophys. Geosystems 5, 1–11. doi:10.1029/2004GC000807

Lund, S.P., 2018. A New View of Long-Term Geomagnetic Field Secular Variation. Front. Earth Sci. 6, 1–13. doi:10.3389/feart.2018.00040

Maisuradze, G.M., Kuloshvili, S.I., 1999. “Some Geological Problems of Late Volcanism in the Dzhavakheti Upland.” Tr. GIN AN Gruz. Nov. Ser. 114, 220–228.

McElhinny, M.W., McFadden, P.L., 1997. Palaeosecular variation over the past 5 Myr based on a new generalized database. Geophys. J. Int. 131, 240–252. doi:10.1111/j.1365-246X.1997.tb01219.x

McElhinny, M.W., McFadden, P.L., Merrill, R.T., 1996. The time-averaged paleomagnetic field 0-5 Ma. J. Geophys. Res. Solid Earth 101, 25007–25027. doi:10.1029/96JB01911

McFadden, P.L., McElhinny, M.W., 1982. Variations in the Geomagnetic Dipole 2: Statistical Analysis of VDMs for the Past 5 Million Years. J. Geomagn. Geoelectr. 34, 163–189. doi:10.5636/jgg.34.163

McFadden, P.L., Merrill, R.. T., McElhinny, M.W., 1988. Dipole / Quadrupole Family Modeling of Paleosecular Variation. J. Geophys. Res. 93, 11583–11588. doi:10.1029/JB093iB10p11583

Merrill, R.T., McElhinny, M.W., McFadden, P.L., 1996. The Magnetic Field of the Earth. Paleomagnetism, the Core, and the Deep Mantle. Academic Perss. International Geophysics Series. Volume 63, San Diego.

Merrill, R.T., Mcfadden, P.L., 2003. The geomagnetic axial dipole field assumption. Phys. Earth Planet. Inter. 139, 171–185. doi:10.1016/j.pepi.2003.07.016

Paterson, G.A., 2013. The effects of anisotropic and non-linear thermoremanent magnetizations on Thellier-type paleointensity data. Geophys. J. Int. 193, 694–710. doi:10.1093/gji/ggt033

Paterson, G.A., 2011. A simple test for the presence of multidomain behavior during paleointensity experiments. J. Geophys. Res. Solid Earth 116, 1–12. doi:10.1029/2011JB008369

Paterson, G.A., Biggin, A.J., Hodgson, E., Hill, M.J., 2015. Thellier-type paleointensity data from multidomain specimens. Phys. Earth Planet. Inter. 245, 117–133. doi:10.1016/j.pepi.2015.06.003

Paterson, G.A., Tauxe, L., Biggin, A.J., Shaar, R., Jonestrask, L.C., 2014a. On improving the selection of Thellier-type paleointensity data Greig. Geochemistry, Geophys. Geosystems 15, 1180–1192. doi:10.1002/2013GC005135

Paterson, G.A., Tauxe, L., Biggin, A.J., Shaar, R., Jonestrask, L.C., 2014b. On improving the selection of Thellier-type paleointensity data. Geochemistry, Geophys. Geosystems 15, 1180–1192. doi:10.1002/2013GC005135

Perrin, M., Shcherbakov, V., 1997. Paleointensity of the Earth's Magnetic Field for the Past 400 Ma: Evidence for a Dipole Structure during the Mesozoic Low. J. Geomagn. Geoelectr. 49, 601–614. doi:10.5636/jgg.49.601

Prévot, M., Derder, M.E.-M., McWilliams, M., Thompson, J., 1990. Intensity of the Earth's magnetic field: Evidence for a Mesozoic dipole low. Earth Planet. Sci. Lett. 97, 129–139. doi:10.1016/0012-821X(90)90104-6

Prévot, M., Mankinen, E.A., Coe, R.S., Grommé, C.S., 1985. The Steens Mountain (Oregon) geomagnetic polarity transition: 2. Field intensity variations and discussion of reversal models. J. Geophys. Res. Solid Earth 90, 10417–10448. doi:10.1029/JB090iB12p10417

Prevot, M., Mankinen, E.A., Gromme, C.S., Coe, R.S., Prévot, M., Mankinen, E.A., Grommé, C.S., Coe, R.S., Prevot, M., Mankinen, E.A., Gromme, C.S., Coe, R.S., Prévot, M., Mankinen, E.A., Grommé, C.S., Coe, R.S., 1985. How the geomagnetic field vector reverses polarity. Nature 316, 230–234. doi:10.1038/316230a0

Riisager, J., Perrin, M., Riisager, P., Ruffet, G., 2000. Paleomagnetism, paleointensity and geochronology of Miocene basalts and baked sediments from Velay Oriental, French Massif Central. J. Geophys. Res. Solid Earth 105, 883–896. doi:10.1029/1999JB900337

Roberts, A.P., Tauxe, L., Heslop, D., Zhao, X., Jiang, Z., 2018. A Critical Appraisal of the "Day" Diagram. J. Geophys. Res. Solid Earth. doi:10.1002/2017JB015247

Sánchez-Moreno, E.M., 2018. Variation of the absolute paleointensity of the Earth's magnetic field recorded in sequences of basaltic flows from the volcanic region of Djavakheti (Georgia). Universidad de Burgos. doi:10.13140/RG.2.2.30939.00804

Sánchez-Moreno, E.M., Calvo-Rathert, M., Goguitchaichvili, A., Vashakidze, G.T., Lebedev, V.A., 2018. Evidence of Unusual Geomagnetic Regimes Recorded in Plio-Pleistocene Volcanic Sequences from the Lesser Caucasus (Southern Georgia). Geochemistry, Geophys. Geosystems 19, 1–18. doi:10.1029/2017GC007358

Santos, C.N., Tauxe, L., 2019. Investigating the Accuracy, Precision, and Cooling Rate Dependence of Laboratory-Acquired Thermal Remanences During Paleointensity Experiments. Geochemistry, Geophys. Geosystems 1–15. doi:10.1029/2018GC007946

Selkin, P.A., Gee, J.S., Tauxe, L., 2007. Nonlinear thermoremanence acquisition and implications for paleointensity data. Earth Planet. Sci. Lett. 256, 81–89. doi:10.1016/j.epsl.2007.01.017

Selkin, P.A., Tauxe, L., 2000. Long-term variations in palaeointensity. Philos. Trans. R. Soc. A Math. Phys. Eng. Sci. 358, 1065–1088. doi:10.1098/rsta.2000.0574

Shaar, R., Tauxe, L., 2013. Thellier GUI: An integrated tool for analyzing paleointensity data from Thellier-type experiments. Geochemistry, Geophys. Geosystems 14, 677–692. doi:10.1002/ggge.20062

Smirnov, A. V., Kulakov, E. V., Foucher, M.S., Bristol, K.E., 2017. Intrinsic paleointensity bias and the long-term history of the geodynamo. Sci. Adv. 3, e1602306. doi:10.1126/sciadv.1602306

Smirnov, A. V., Tarduno, J.A., 2003a. Magnetic hysteresis monitoring of Cretaceous submarine basaltic glass during Thellier paleointensity experiments: evidence for alteration and attendant low field bias. Earth Planet. Sci. Lett. 206, 571–585. doi:10.1016/S0012-821X(02)01123-8

Smirnov, A. V., Tarduno, J.A., 2003b. Magnetic hysteresis monitoring of Cretaceous submarine basaltic glass during Thellier paleointensity experiments: Evidence for alteration and attendant low field bias. Earth Planet. Sci. Lett. 206, 571–585. doi:10.1016/S0012-821X(02)01123-8

Tanaka, H., Kobayashi, T., 2003. Paleomagnetism of the late Quaternary Ontake Volcano , Japan : directions , intensities , and excursions. Earth, Planets Sp. 55, 189–202. doi:10.1186/BF03351748

Tanaka, H., Kono, M., Kaneko, S., 1995. Paleosecular Variation of Direction and Intensity from Two Pliocene-Pleistocene Lava Sections in Southwestern Iceland. J. Geomagn. Geoelectr. 47, 89–102. doi:10.5636/jgg.47.89

Tarduno, J.A., Cottrell, R.D., Davis, W.J., Nimmo, F., Bono, R.K., 2015. A Hadean to Paleoarchean geodynamo recorded by single zircon crystals. Science (80-.). 349, 521–524. doi:10.1126/science.aaa9114

Tauxe, L., 2006. Long-term trends in paleointensity: The contribution of DSDP/ODP submarine basaltic glass collections. Phys. Earth Planet. Inter. 156, 223–241. doi:10.1016/j.pepi.2005.03.022

Tauxe, L., Gans, P., Mankinen, E.A., 2004. Paleomagnetism and 40Ar/39Ar ages from volcanics extruded during the Matuyama and Brunhes Chrons near McMurdo Sound, Antarctica. Geochemistry, Geophys. Geosystems 5, 1–20. doi:10.1029/2003GC000656

Tauxe, L., Gee, J.S., Steiner, M.B., Staudigel, H., 2013. Paleointensity results from the Jurassic: New constraints from submarine basaltic glasses of ODP Site 801C. Geochemistry, Geophys. Geosystems 14, 4718–4733. doi:10.1002/ggge.20282

Tauxe, L., Shaar, R., Jonestrask, L., Swanson-Hysell, N.L., Minnett, R., Koppers, A.A.P., Constable, C.G., Jarboe, N., Gaastra, K., Fairchild, L., 2016. PmagPy: Software package for paleomagnetic data analysis and a bridge to the Magnetics Information Consortium (MagIC) Database. Geochemistry, Geophys. Geosystems 17, 2450–2463. doi:10.1002/2016GC006307

Tauxe, L., Staudigel, H., 2004. Strength of the geomagnetic field in the cretaceous normal superchron: New data from submarine basaltic glass of the troodos ophiolite. Geochemistry, Geophys. Geosystems 5, 223–241. doi:10.1029/2003GC000635

Thellier, E., Thellier, O., 1959. Sur líntensité du champ magnétique terrestre dans le passé historique et géologique. Ann. Geophys. 15, 285–376.

Valet, J.-P., Meynadier, L., Guyodo, Y., 2005. Geomagnetic dipole strength and reversal rate over the past two million years. Nature 435, 802–805. doi:10.1038/nature03674

Valet, J.P., Meynadier, L., Guyodo, Y., 2005. Geomagnetic dipole strength and reversal

rate over the past two million years. Nature 435, 802–805. doi:10.1038/nature03674
Wang, H., Kent, D. V., Rochette, P., 2015. Weaker axially dipolar time-averaged paleomagnetic field based on multidomain-corrected paleointensities from Galapagos lavas. Proc. Natl. Acad. Sci. 112, 15036–15041. doi:10.1073/pnas.1505450112
Yamamoto, Y., Tsunakawa, H., 2005. Geomagnetic field intensity during the last 5 Myr: LTD-DHT Shaw palaeointensities from volcanic rocks of the Society Islands, French Polynesia. Geophys. J. Int. 162, 79–114. doi:10.1111/j.1365-246X.2005.02651.x
Yu, Y., Tauxe, L., 2005. Testing the IZZI protocol of geomagnetic field intensity determination. Geochemistry, Geophys. Geosystems 6. doi:10.1029/2004GC000840
Yu, Y., Tauxe, L., Genevey, A., 2004. Toward an optimal geomagnetic field intensity determination technique. Geochemistry, Geophys. Geosystems 5, n/a-n/a. doi:10.1029/2003GC000630
Zijderveld, J.D.A., 1967. A. C. Demagnetization of Rocks: Analysis of Results. Dev. Solid Earth Geophys. 3, 254–286. doi:10.1016/B978-1-4832-2894-5.50049-5

Table 1: Successful paleointensity determinations obtained with the TT and IZZI methods. *site:* Lava flow name. *spec.*: Specimen sub-name. *meth.:* paleointensity determination method. *Tmin, Tmax*: Minimum and maximum temperature used for the determination. B_{anc}: Paleointensity value. *n:* Number of experiment steps used in the determination. Experimental statistics: *FRAC, β, gmax, |k'|, MAD, DANG,* $n_{pTRM\ checks}$ (see the Standard Paleointensity Definitions (Paterson et al., 2014)).

site	spec.	meth.	Tmin (°C)	Tmax (°C)	B_{anc} (uT)	σB_{anc} (µT)	n	β	frac	gmax	|k'|	MAD	DANG	$n_{pTRM-checks}$
AP01	06B3	IZZI	450	600	38.3	0.8	9	0.02	0.62	0.3	0.027	3.0	1.3	5
AP04	01B3	IZZI	450	580	33.3	2.3	5	0.07	0.61	0.4	0.268	2.6	1.2	4
AP04	01C3	IZZI	450	600	31.9	0.3	9	0.01	0.69	0.3	0.000	3.2	1.8	5
AP04	02B3	IZZI	500	600	34.3	0.7	7	0.02	0.60	0.3	0.026	5.3	1.5	5
AP04	02B4	IZZI	500	600	34.5	1.0	5	0.03	0.63	0.3	0.106	4.6	2.3	4
AP04	03B3	TT	0	582	26.6	1.3	10	0.05	0.97	0.2	0.296	11.5	8.3	4
AP07	03B3	IZZI	400	600	18.0	0.7	10	0.04	0.65	0.3	0.139	5.8	4.8	5
AP07	06B4	IZZI	450	580	18.7	0.7	5	0.04	0.64	0.4	0.191	5.7	4.9	4
AP11	01B3	IZZI	400	600	29.3	0.9	10	0.03	0.62	0.3	0.277	8.3	3.6	5
AP11	01B5	IZZI	450	600	28.9	1.7	6	0.06	0.63	0.4	0.286	3.9	3.2	4
AP11	03A4	IZZI	350	600	22.2	0.9	8	0.04	0.72	0.3	0.299	5.3	5.1	4
AP14	01A3	IZZI	300	600	19.1	0.4	12	0.02	0.75	0.2	0.064	6.6	2.7	5
AP14	03A3	IZZI	300	570	19.8	0.4	10	0.02	0.71	0.2	0.163	4.2	3.9	4
AP14	04B3	IZZI	200	525	19.8	0.2	8	0.01	0.61	0.2	0.045	8.3	7.6	3
AP14	05B3	TT	142	582	20.5	0.6	11	0.03	0.84	0.2	0.050	8.9	9.0	5
AP14	06B3	TT	351	582	20.1	1.0	9	0.05	0.61	0.2	0.250	11.6	6.7	5
AP14	07B3	IZZI	200	525	19.9	0.2	8	0.01	0.64	0.2	0.064	8.7	3.9	3
AP14	08B3	IZZI	0	600	19.8	0.4	14	0.02	0.96	0.2	0.014	5.3	1.7	5
AP14	08B4	IZZI	350	600	19.4	0.8	8	0.04	0.65	0.3	0.065	2.1	2.1	4
AP16	03B3	IZZI	0	500	54.7	3.8	8	0.07	0.66	0.3	0.127	11.4	9.4	2

AP16	05B3	IZZI	0	500	51.8	3.1	8	0.06	0.68	0.3	0.167	11.6	9.2	2
AP16	07A3	IZZI	350	600	17.9	0.4	11	0.02	0.61	0.2	0.159	8.7	5.8	5
AP16	07A4	IZZI	350	600	18.7	0.6	8	0.03	0.67	0.3	0.129	4.2	4.4	4
AP16	07A5	IZZI	350	600	18.9	0.2	8	0.01	0.72	0.2	0.047	5.2	3.3	4
AP16	07B3	IZZI	350	600	14.8	0.9	8	0.06	0.63	0.3	0.270	3.5	2.8	4
AP16	07B4	IZZI	350	600	13.7	0.7	8	0.05	0.63	0.2	0.232	7.7	6.2	4
AP17	01B3	IZZI	400	600	25.7	0.5	10	0.02	0.61	0.2	0.217	7.9	3.9	5
AP17	01B4	IZZI	400	600	27.9	1.1	7	0.04	0.65	0.3	0.284	7.1	4.0	4
AP17	01B5	IZZI	400	600	25.9	1.0	7	0.04	0.62	0.3	0.239	6.1	2.3	4
AP17	04B3	IZZI	300	600	20.3	0.6	12	0.03	0.78	0.2	0.247	9.6	5.8	5
AP17	04B4	IZZI	400	600	18.7	0.9	7	0.05	0.67	0.3	0.296	8.7	7.1	4
AP17	08B3	IZZI	350	580	17.8	0.7	10	0.04	0.62	0.2	0.297	7.0	8.7	5
AP18	02B3	TT	351	582	24.7	0.5	9	0.02	0.63	0.3	0.039	9.8	9.6	5
AP18	03B3	IZZI	300	600	24.3	0.5	12	0.02	0.63	0.2	0.138	8.7	5.1	5
AP18	05B3	IZZI	300	580	23.6	0.9	11	0.04	0.75	0.2	0.299	8.8	7.7	5
AP18	05B4	IZZI	350	560	23.7	1.2	6	0.05	0.64	0.3	0.293	5.4	5.8	3
AP18	05B5	IZZI	350	560	24.0	1.4	6	0.06	0.61	0.3	0.238	3.1	2.5	3
AP19	02B3	IZZI	350	600	20.1	0.6	11	0.03	0.87	0.2	0.172	5.5	3.5	5
AP19	03B3	IZZI	475	580	21.1	0.6	7	0.03	0.62	0.3	0.000	3.6	3.1	5
AP19	05B3	IZZI	500	600	21.2	0.0	7	0.00	0.61	0.4	0.009	4.3	2.9	5
AP19	07A3	IZZI	450	580	21.9	0.7	8	0.03	0.62	0.3	0.144	5.5	2.3	5
AP19	07A4	IZZI	500	600	20.7	0.8	5	0.04	0.61	0.4	0.177	6.7	4.9	4
AP20	01B3	IZZI	350	570	19.4	0.8	9	0.04	0.63	0.2	0.266	7.7	6.0	4
AP20	04A3	IZZI	200	550	19.4	0.8	9	0.04	0.72	0.2	0.274	7.6	9.6	3
AP20	06A3	IZZI	300	560	19.4	0.8	9	0.04	0.65	0.2	0.220	6.2	6.3	4

Table 2: Averaged paleointensity by lava flow results. *site:* Lava flow name. *polarity:* VGP polarity obtained to each lava flow. *min age:* K-Ar date obtained from the flows AP01 and AP12. B_{anc}: Paleointensity value. σ_{site}: Standard deviation by site. *VADM:* Virtual axis dipole moment.

site	polarity	min age (Ma)	B (μT)	n_{SITE}	σ_{SITE} (μT)	σ_{SITE} (%)	VADM (ZAm^2)	σVADM (ZAm^2)
AP04	N	3.09	32.1	5	3.3	10.1	54.6	5.5
AP11	R	3.70	26.8	3	4.0	14.8	45.6	6.7
AP14	R	3.70	19.8	8	0.4	2.2	33.7	0.7
AP16	R	3.70	16.8	5	2.4	14.3	28.6	4.1
AP17	R	3.70	22.7	6	4.3	18.9	38.7	7.3
AP18	R	3.70	24.1	5	0.4	1.8	40.9	0.7
AP19	R	3.70	21.0	5	0.7	3.2	35.7	1.1
AP20	R	3.70	19.4	3	0.0	0.1	33.0	0.0

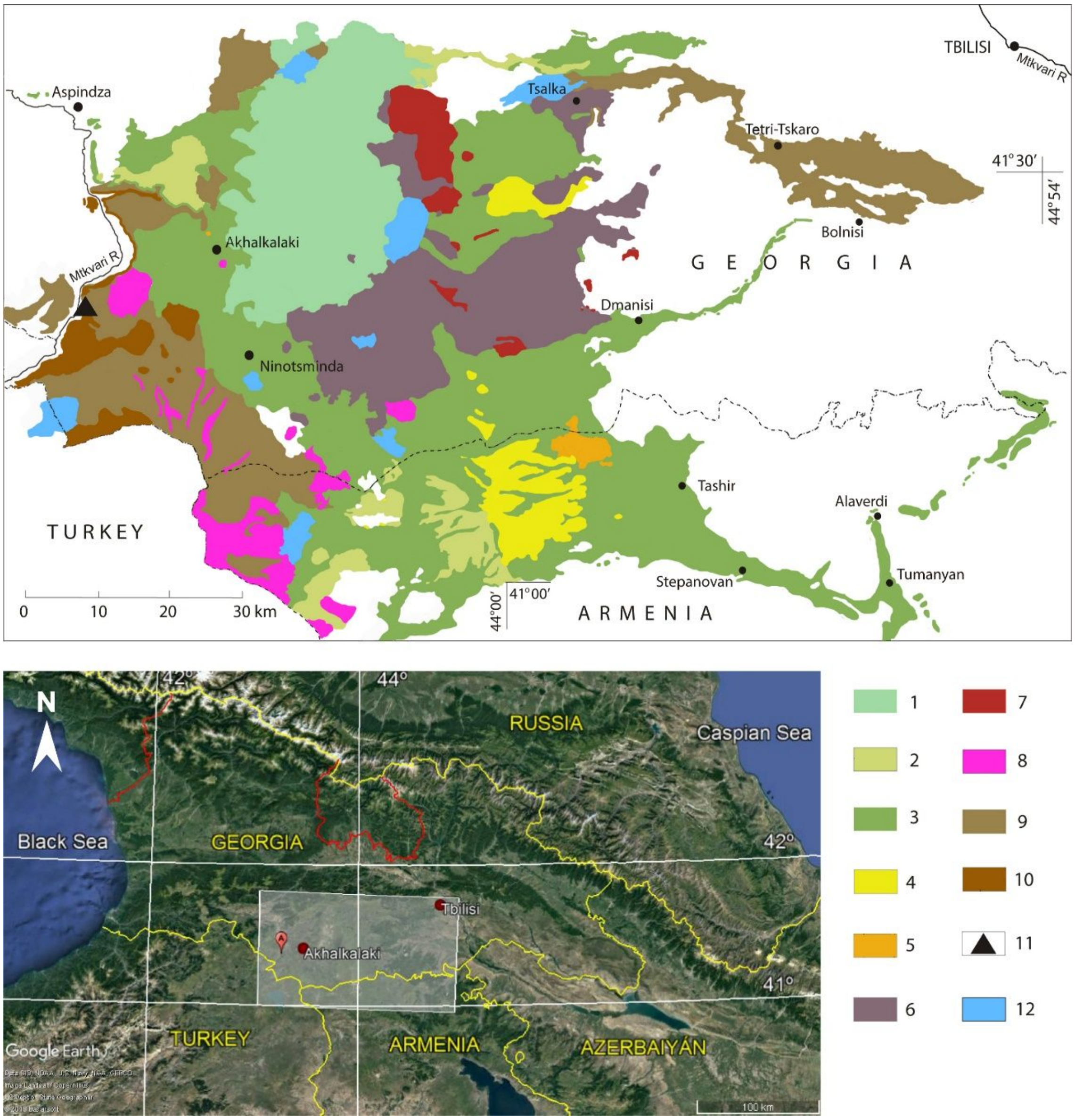

Figure 1. Schematic geological map of the Plio-Pleistocene magmatism in the Djavakheti Highland (Lesser Caucasus) showing lava flow sequences sampled in the present study (taken from Sánchez-Moreno et al., 2018; and modified from Lebedev et al., 2008; Lebedev, 2015). 1 - Quaternary volcanic rocks (andesites and dacites) of the Samsari ridge (800 – 0 ka); 2-10 Pliocene – Early Quaternary volcanic rocks of Akhalkalaki formation: 2 - Basic lavas (1.75 – 1.40 Ma), 3 - Basic lavas (2.15 – 1.95 Ma), 4 - Later dacites and rhyolites of the Javakheti ridge (2.25 Ma), 5 - Hyalodacite (2.5 Ma), 6 - Basic lavas (2.65 – 2.45 Ma), 7 - Earlier rhyolites and dacites of the Djavakheti ridge (2.85 – 2.6 Ma), 8 - Dacites of the SW part of Djavakheti highland (3.15 – 3.11 Ma), 9 - Basic lavas (3.22 – 3.04 Ma), 10 - Basic lavas (3.75 – 3.55 Ma), 11 - Sampled lava flow sequences of Apnia, 12 - Lakes. Location map from Google Earth: Image Landsat/Copernicus © 2018 Basarsoft, US Dept. of State Geographer.

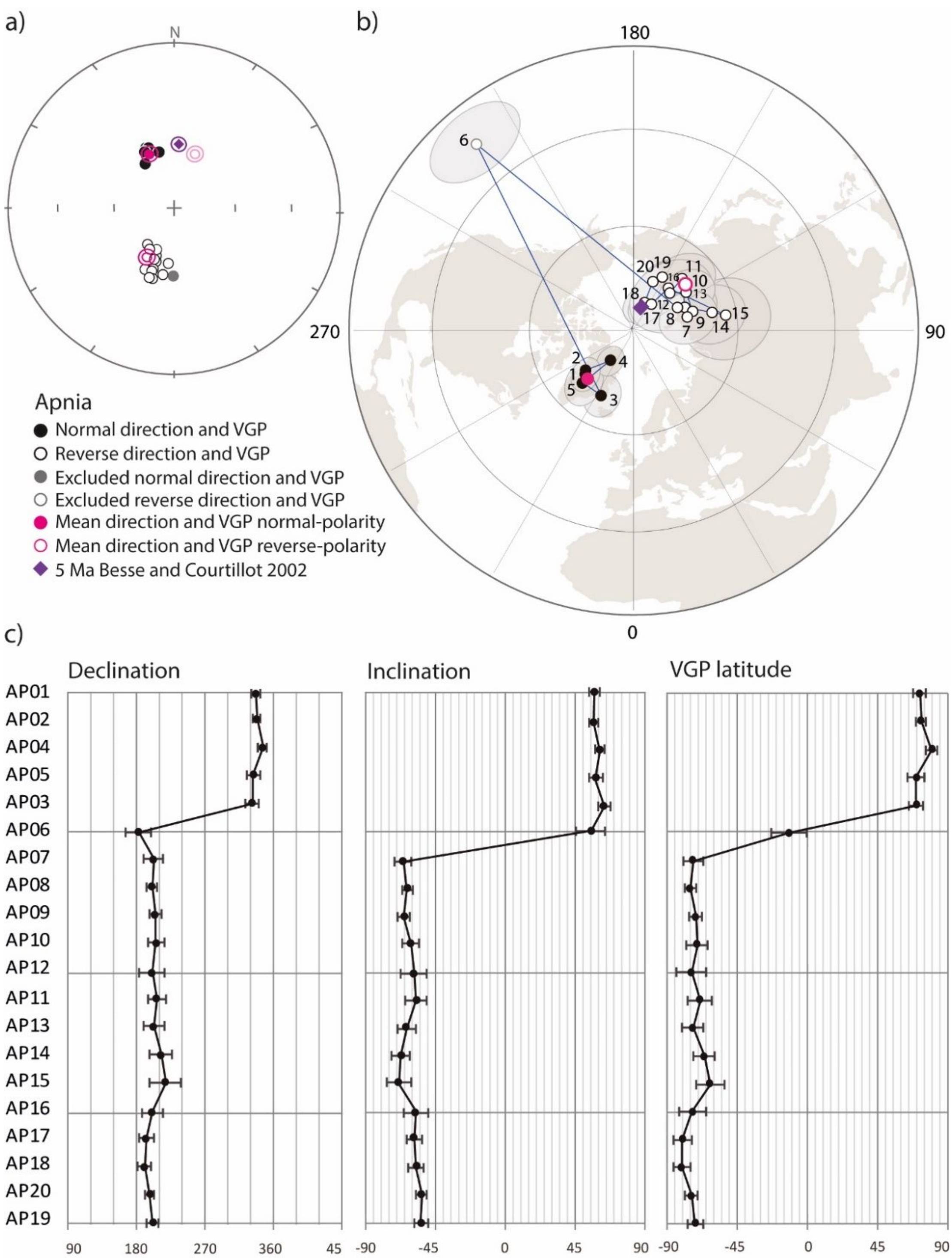

Figure 2. Paleomagnetic results of the Apnia sequence (Sánchez-Moreno et al., 2018). (a) Stereographic projection of mean paleomagnetic directions (ChRMs) of each lava flow. Normal and reverse directions averages and their α_{95} in pink (reverse average is projected in both north and south hemispheres). Expected direction (Besse and Courtillot, 2002) in purple. (b) Stereographic projection of Virtual Geomagnetic Poles. Normal and reverse polarities averages in pink. Expected pole for the last 5 Ma in Eurasia (Besse and Courtillot, 2002) in purple. (c) Declination and inclination of paleomagnetic directions, and VGP latitudes, stratigraphically ordered. Figure taken from Sánchez-Moreno et al. 2018.

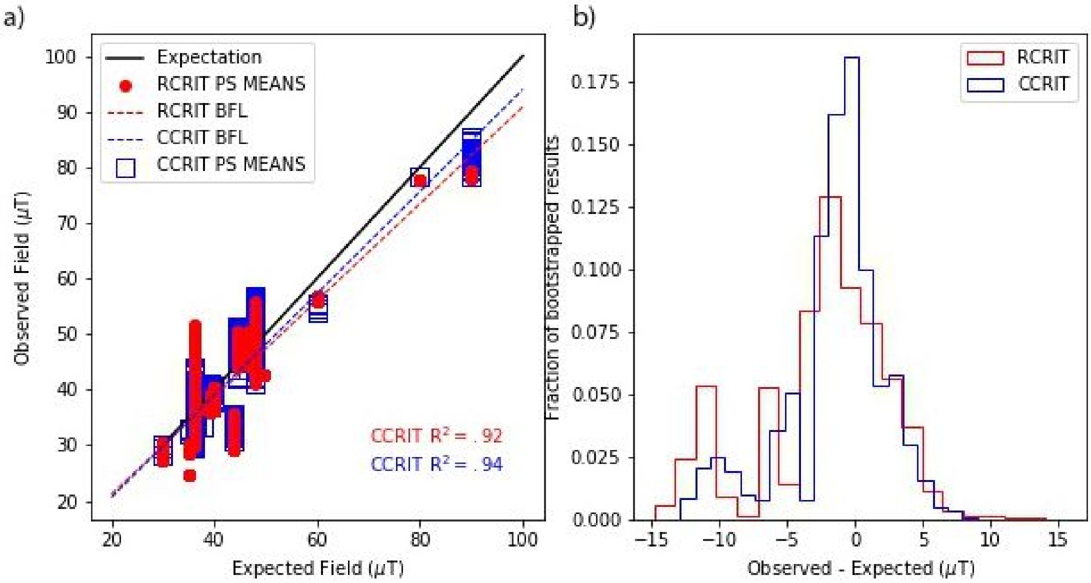

Figure 3: Comparison of estimated intensity values using the sets of selection criteria CCRIT and its relaxed version RCRIT for 1000 bootstrapped samples of data set from specimens that cooled in a historical or laboratory field (Tauxe et al., 2016). The R^2 values of the linear regressions are shown. CCRIT and RCRIT both perform reasonably well, with CCRIT slightly better than the more relaxed set of criteria.

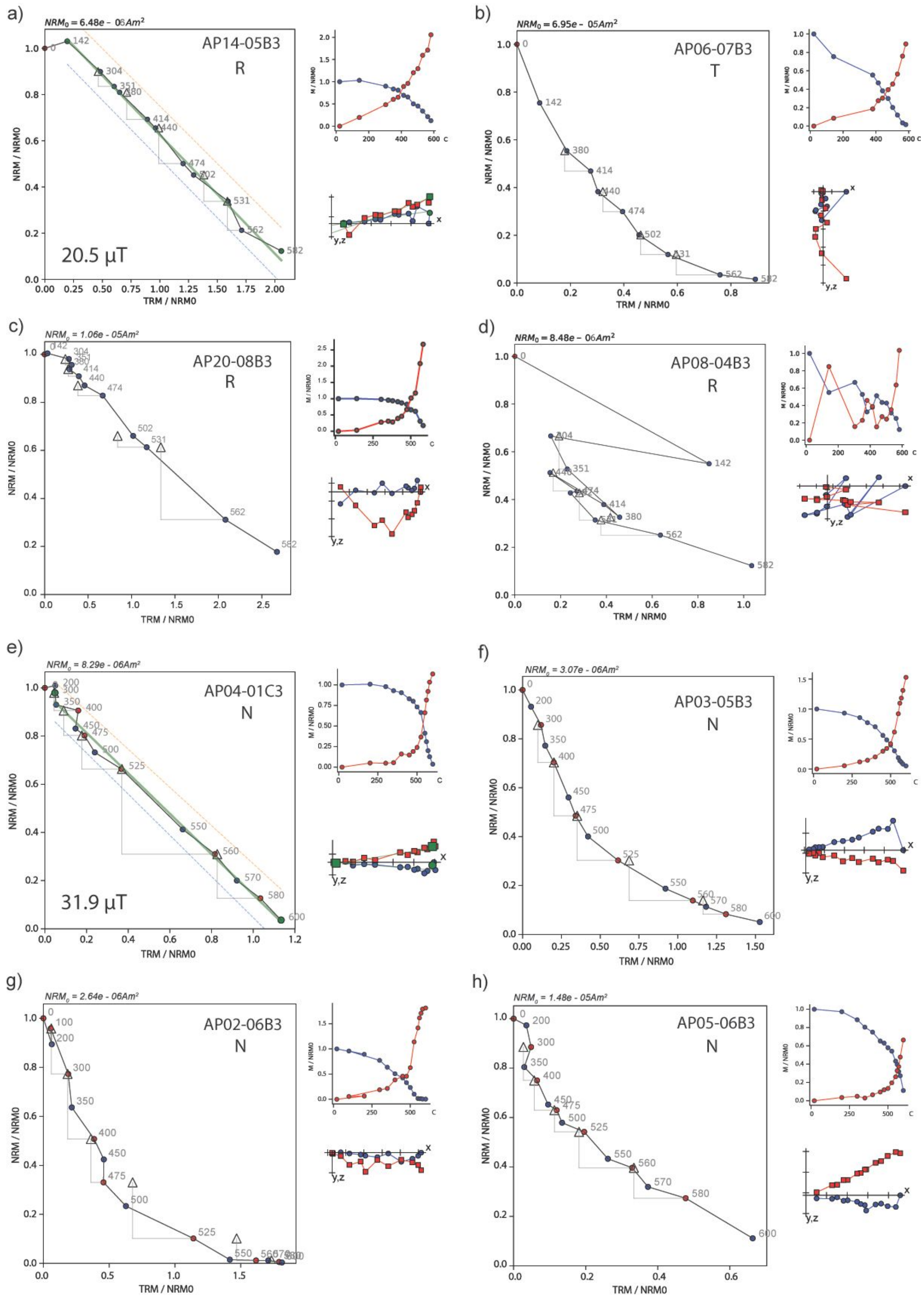

Figure 4: Representative Thellier-Thellier and IZZI experiments. Different behaviors are shown for TT (a-d) and IZZI (f-i): Successful determinations (a and e), passed the RCRIT acceptance criteria and the best fit line is shown in solid green. The SCAT criterion is plotted as dotted lines. Failing determination by the curvature (b and f), determination with magnetochemical alteration (c and f), no orientation kept during measurements (d)

and zig-zag behaviour of the MD (h). Upper figures are the Arai plots (Nagata et al., 1963). Lower-right ones are the Zijderveld plots (Zijderveld, 1967). The blue circles are horizontal projections of the zero field steps after adjusting the NRM value of x to be zero, red squares are the X and Z vertical projections. Lower-left figures are the magnetizations remaining (blue) and gained (red) at each temperature step. N: Paleointensity from normal polarity lava flow. R: reverse polarity. T: Transitional polarity.

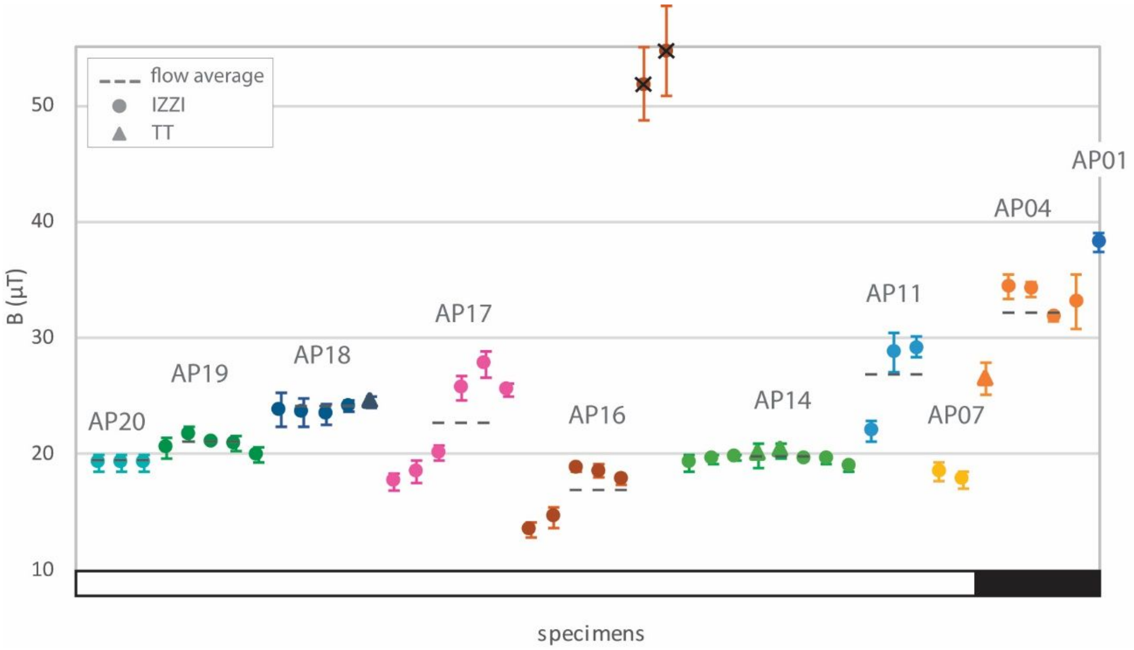

Figure 5: Plot of specimen data by lava flow. Triangles (circles) are the IZZI (Thellier-Thellier) results. Individual results crossed out have been dismissed. Flow means are plotted as dotted lines.

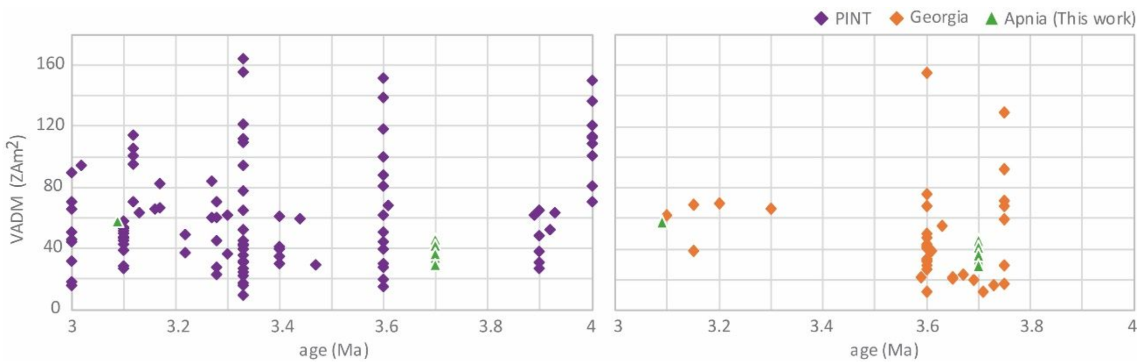

Figure 6. VADM calculated from paleointensities between 3 and 4 Ma (age range covered by the Apnia sequence), extracted from the PINT2015.05 database (Biggin et al., 2010). a) VADM from different latitudes, excluding Georgia data, plotted together with Apnia results from the present study. b) VADM from the Djvakheti Highland plotted together with Apnia results from the present study.

Supplementary material

Weak paleointensity results over a Pliocene volcanic sequence from Lesser Caucasus (Georgia): Transitional record or time averaged field?

Elisa M. Sánchez-Moreno[1,*], Manuel Calvo-Rathert[1,2], Avto Goguitchaichvili[3], Lisa Tauxe[4], George T. Vashakidze[5], Vladimir A. Lebedev[6]

[1]Departamento de Física, EPS Campus Rio Vena – Universidad de Burgos, Av. Cantabria, s/n, 09006 Burgos, Spain.
[2]Hawaii Institute of Geophysics and Planetology, University of Hawaii at Manoa, Honolulu, HI, United States
[3]Laboratorio Interinstitucional de Magnetismo Natural, Instituto de Geofísica Unidad Michoacán, UNAM – Campus Morelia, 58990 Morelia, México.
[4]Scripps Institution of Oceanography, University of California - San Diego, La Jolla, CA 92093-0220, USA.
[5]Alexandre Janelidze Institute of Geology – Ivane Javakhishvili Tbilisi State University, 1/9 M. Alexidze str., 0171 Tbilisi, Georgia.
[6]Institute of Geology of Ore Deposits, Petrography, Mineralogy and Geochemistry – Russian Academy of Sciences (IGEM RAS), Staromonetny per., 35, 119017 Moscow, Russia.

*Corresponding author, Elisa M. Sánchez-Moreno: emsanchez@ubu.es

Figures

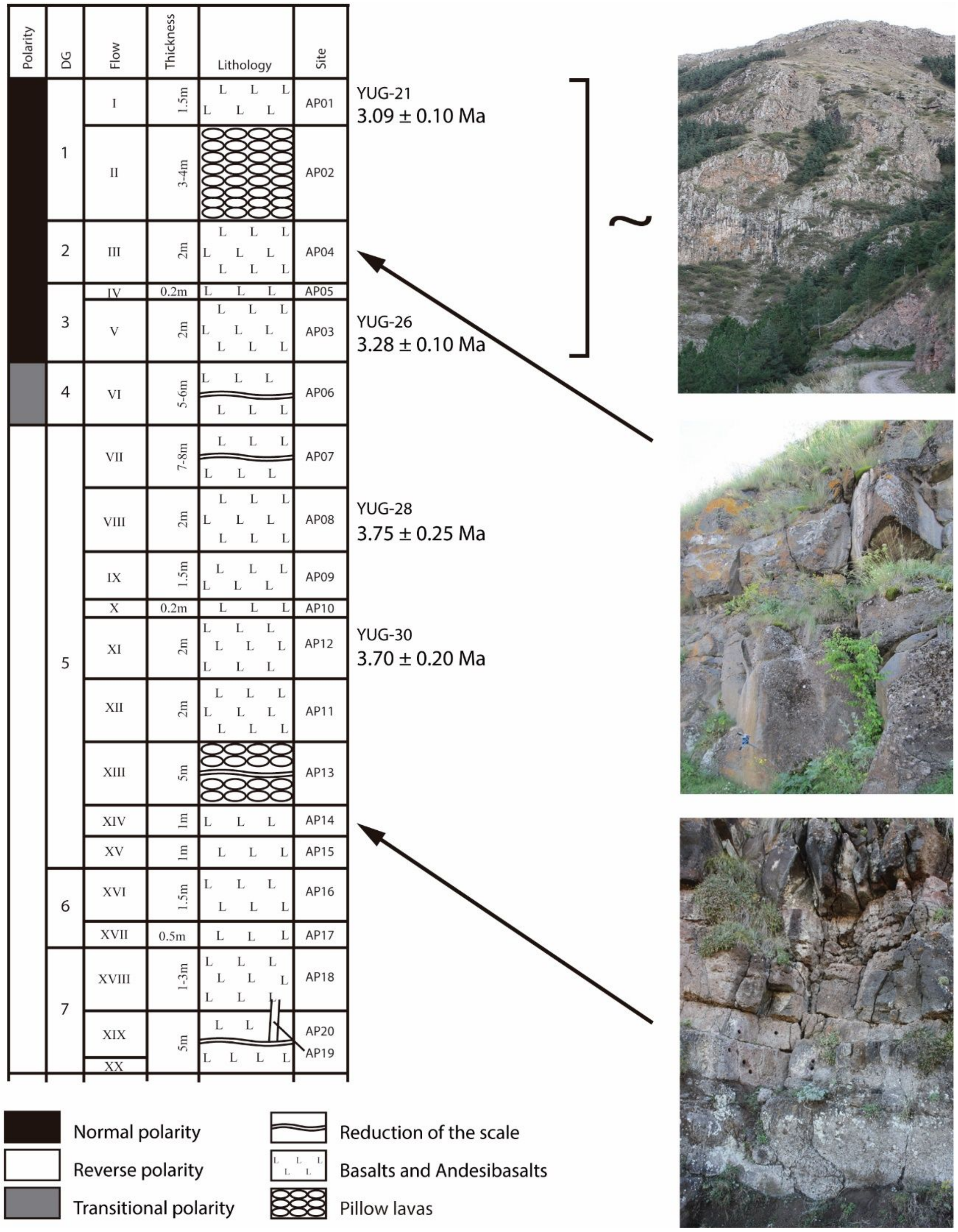

Figure S1. Schematic stratigraphic column of the Apnia sequence (location in Fig. 1.). K-Ar datings from Lebedev et al. (2008). Polarity and Directional Groups (DG) are shown. The first image corresponds roughly to the lava flows of the upper section of the normal polarity sequence. The second ones are AP04 and AP14 flows respectively. Modified after Sanchez-Moreno et al., 2018.

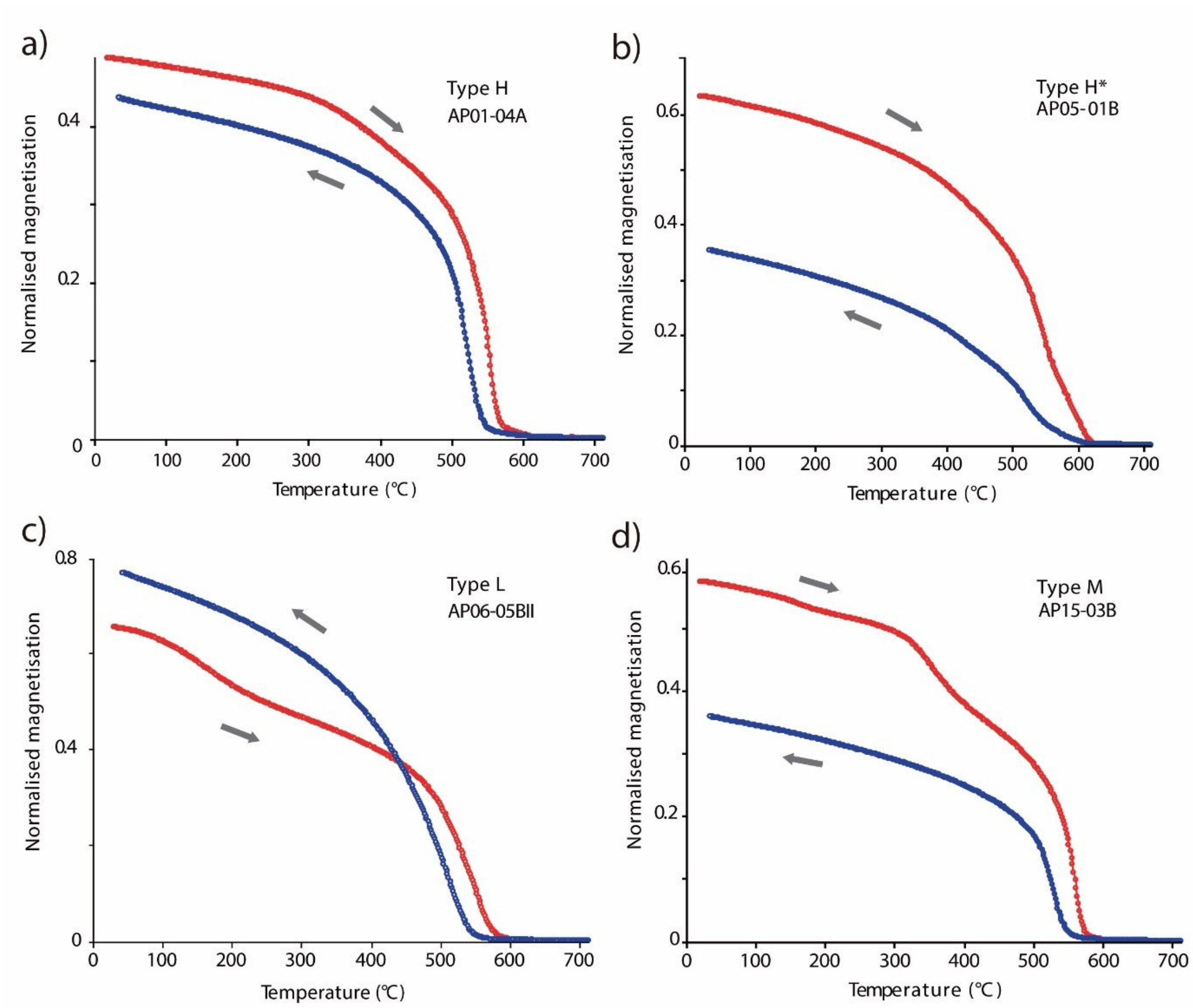

Figure S2. Normalized strong field magnetization versus temperature curves (Ms-T) of representative samples (modified after Sánchez-Moreno et al., 2018). The arrows indicate the heating and cooling curves. Curve types are discussed in the text.

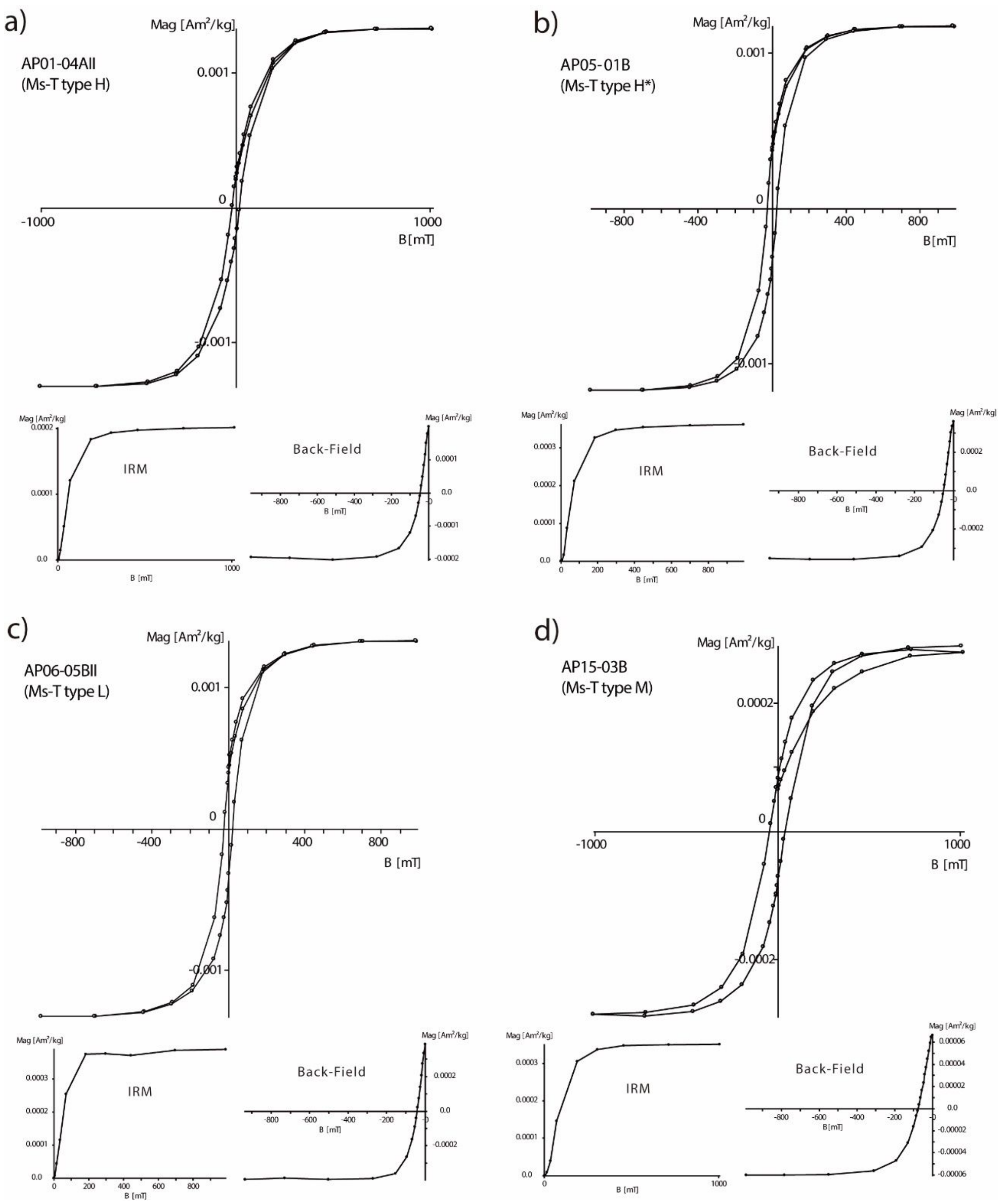

Figure S3. Examples of hysteresis loops (corrected) and their corresponding IRM acquisition curves and back-field curves of samples from the Apnia sequence. These examples correspond to the same samples shown as types of thermomagnetic curves (M_S-T) examples in Fig. S2.

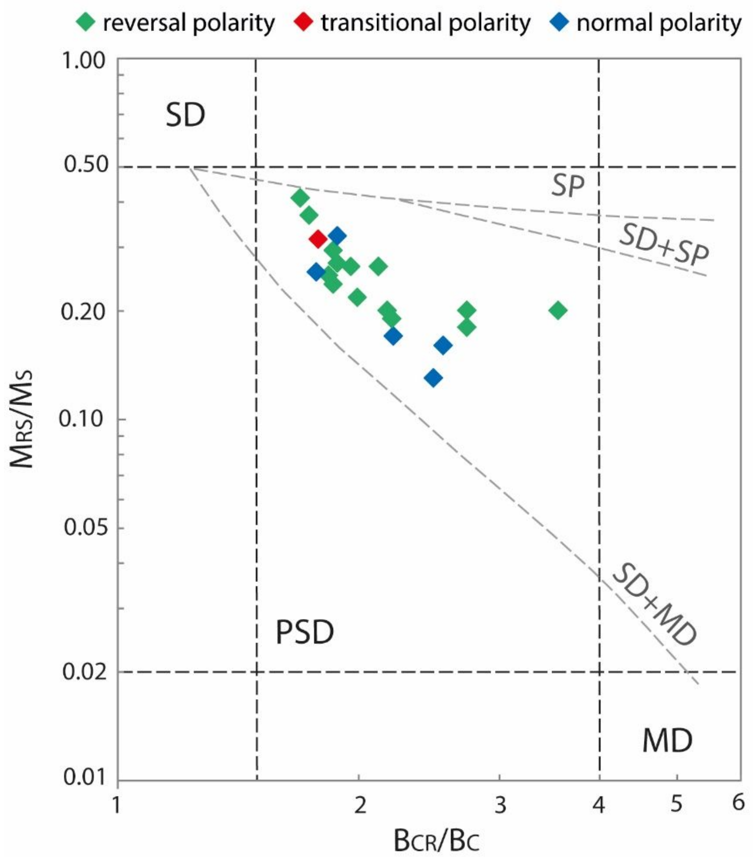

Figure S4. Bi-logarithmic Day-plot (Day et al., 1977) modified after (Dunlop, 2002). M_{RS}/M_S: Saturation remanence to saturation magnetization. B_{CR}/B_{C}: Coercivity of remanence to coercivity.

Tables

lat (°N)	VADM (ZAm²)	age (Ma)	references	lat (°N)	VADM (ZAm²)	age (Ma)	references
PINT 3-4 Ma T+				**PINT 3-4 Ma T+**			
21.40	50.28	3.00	Coe et al. (1984)	21.25	30.21	3.33	Herrero-Bervera and Valet (2005)
21.40	89.63	3.00	Coe et al. (1984)	21.25	42.46	3.33	Herrero-Bervera and Valet (2005)
21.40	15.30	3.00	Coe et al. (1984)	21.25	77.7	3.33	Herrero-Bervera and Valet (2005)
21.40	17.49	3.00	Coe et al. (1984)	21.25	39.4	3.33	Herrero-Bervera and Valet (2005)
21.40	19.67	3.60	Coe et al. (1984)	21.25	155.4	3.33	Herrero-Bervera and Valet (2005)
21.40	50.28	3.60	Coe et al. (1984)	21.25	120.8	3.33	Herrero-Bervera and Valet (2005)
21.40	87.44	3.60	Coe et al. (1984)	21.25	111.6	3.33	Herrero-Bervera and Valet (2005)
21.40	43.72	3.60	Coe et al. (1984)	21.25	109.4	3.33	Herrero-Bervera and Valet (2005)
21.40	45.91	3.00	Coe et al. (1984)	21.25	41.59	3.33	Herrero-Bervera and Valet (2005)
36.90	48.39	3.90	Juarez and Tauxe (2000)	21.25	15.54	3.33	Herrero-Bervera and Valet (2005)
36.90	30.47	3.90	Juarez and Tauxe (2000)	21.25	31.08	3.33	Herrero-Bervera and Valet (2005)
36.90	26.89	3.90	Juarez and Tauxe (2000)	21.25	26.7	3.33	Herrero-Bervera and Valet (2005)
36.90	37.64	3.90	Juarez and Tauxe (2000)	21.25	164.2	3.33	Herrero-Bervera and Valet (2005)
9.00	29.95	3.40	Juarez and Tauxe (2000)	21.25	94.12	3.33	Herrero-Bervera and Valet (2005)
9.00	34.94	3.40	Juarez and Tauxe (2000)	21.25	45.09	3.33	Herrero-Bervera and Valet (2005)
23.00	51.40	3.10	Juarez and Tauxe (2000)	21.25	35.46	3.33	Herrero-Bervera and Valet (2005)
23.00	53.54	3.10	Juarez and Tauxe (2000)	37.00	61.58	3.60	Tauxe (2006)
23.00	49.26	3.10	Juarez and Tauxe (2000)	37.00	29.72	3.60	Tauxe (2006)
23.00	57.82	3.10	Juarez and Tauxe (2000)	37.00	14.5	3.60	Tauxe (2006)
23.00	44.97	3.10	Juarez and Tauxe (2000)	37.00	30.08	3.60	Tauxe (2006)
23.00	42.83	3.10	Juarez and Tauxe (2000)	37.00	27.39	3.60	Tauxe (2006)
23.00	27.84	3.10	Juarez and Tauxe (2000)	37.00	39.21	3.60	Tauxe (2006)
23.00	51.40	3.10	Juarez and Tauxe (2000)	-16.47	67.76	3.61	Yamamoto and Tsunakawa (2005)
23.00	47.12	3.10	Juarez and Tauxe (2000)	27.25	43.74	3.00	Morales et al. (2003)
21.56	70.43	3.12	Laj et al. (2000)	27.30	31.18	3.00	Morales et al. (2003)
21.56	114.30	3.12	Laj et al. (2000)	26.00	70.23	3.00	Morales et al. (2003)
21.56	100.30	3.12	Laj et al. (2000)	26.42	65.15	3.00	Morales et al. (2003)
21.56	94.85	3.12	Laj et al. (2000)	-78.21	59.51	3.44	Tauxe et al. (2004a)
21.56	105.10	3.12	Laj et al. (2000)	42.60	60.58	3.40	Tauxe et al. (2004b)
21.56	63.01	3.13	Laj et al. (2000)	-77.69	28.68	3.47	Lawrence et al. (2009)
21.56	65.63	3.16	Laj et al. (2000)	**Georgia**			
21.56	82.20	3.17	Laj et al. (2000)	41.48	12.23	3.60	Camps et al. (1996)
21.56	66.29	3.17	Laj et al. (2000)	41.48	75.78	3.60	Camps et al. (1996)
21.57	93.76	3.02	Laj et al. (2000)	41.48	32.62	3.60	Camps et al. (1996)
21.57	90.49	2.99	Laj et al. (2000)	41.48	47.24	3.60	Camps et al. (1996)
21.58	36.63	3.22	Laj et al. (2000)	41.48	42.48	3.60	Camps et al. (1996)
21.58	48.62	3.22	Laj et al. (2000)	41.48	31.60	3.60	Camps et al. (1996)
21.49	62.88	3.93	Laj et al. (2000)	41.48	40.61	3.60	Camps et al. (1996)
21.49	52.18	3.92	Laj et al. (2000)	41.48	27.02	3.60	Camps et al. (1996)
21.49	64.41	3.90	Laj et al. (2000)	41.48	33.13	3.60	Camps et al. (1996)
21.49	61.79	3.89	Laj et al. (2000)	41.48	43.33	3.60	Camps et al. (1996)
21.44	60.33	3.27	Laj et al. (2000)	41.48	155.10	3.60	Camps et al. (1996)
21.44	83.94	3.27	Laj et al. (2000)	41.48	29.23	3.60	Camps et al. (1996)
21.44	44.81	3.28	Laj et al. (2000)	41.48	68.31	3.60	Camps et al. (1996)
21.44	36.07	3.30	Laj et al. (2000)	41.48	31.60	3.60	Camps et al. (1996)
21.44	61.43	3.30	Laj et al. (2000)	41.48	33.47	3.60	Camps et al. (1996)
21.49	22.49	3.28	Laj et al. (2000)	41.48	29.23	3.60	Camps et al. (1996)
21.49	60.04	3.28	Laj et al. (2000)	41.48	41.29	3.60	Camps et al. (1996)
21.49	27.73	3.28	Laj et al. (2000)	41.48	49.79	3.60	Camps et al. (1996)
21.49	70.52	3.28	Laj et al. (2000)	41.48	42.82	3.60	Camps et al. (1996)
23.00	53.11	3.10	Tauxe (2006)	41.43	62.05	3.10	Calvo-Rathert et al. (2011)
23.00	46.47	3.10	Tauxe (2006)	41.43	69.54	3.20	Calvo-Rathert et al. (2011)

23.00	38.55	3.10	Tauxe (2006)
23.00	27.84	3.10	Tauxe (2006)
23.00	26.98	3.10	Tauxe (2006)
23.00	50.97	3.10	Tauxe (2006)
2.00	49.56	3.10	Tauxe (2006)
19.00	136.10	4.00	Bogue and Paul (1993)
19.00	113.50	4.00	Bogue and Paul (1993)
19.00	100.70	4.00	Bogue and Paul (1993)
19.00	108.80	4.00	Bogue and Paul (1993)
19.00	80.64	4.00	Bogue and Paul (1993)
19.00	120.70	4.00	Bogue and Paul (1993)
19.00	112.40	4.00	Bogue and Paul (1993)
19.00	150.00	4.00	Bogue and Paul (1993)
19.00	108.30	4.00	Bogue and Paul (1993)
19.00	70.05	4.00	Bogue and Paul (1993)
9.00	40.93	3.40	Tauxe (2006)
9.00	39.19	3.40	Tauxe (2006)
17.91	42.46	3.70	Tauxe (2006)
21.25	151.70	3.60	Herrero-Bervera and Valet (2005)
21.25	138.80	3.60	Herrero-Bervera and Valet (2005)
21.25	100.00	3.60	Herrero-Bervera and Valet (2005)
21.25	80.98	3.60	Herrero-Bervera and Valet (2005)
21.25	118.20	3.60	Herrero-Bervera and Valet (2005)
21.25	21.89	3.33	Herrero-Bervera and Valet (2005)
21.25	24.51	3.33	Herrero-Bervera and Valet (2005)
21.25	26.48	3.33	Herrero-Bervera and Valet (2005)
21.25	64.79	3.33	Herrero-Bervera and Valet (2005)
21.25	51.66	3.33	Herrero-Bervera and Valet (2005)
21.25	16.85	3.33	Herrero-Bervera and Valet (2005)
21.25	8.97	3.33	Herrero-Bervera and Valet (2005)
41.43	66.82	3.30	Calvo-Rathert et al. (2011)
41.37	129.50	3.75	Calvo-Rathert et al. (2013)
41.37	59.54	3.75	Calvo-Rathert et al. (2013)
41.37	71.45	3.75	Calvo-Rathert et al. (2013)
41.37	29.43	3.75	Calvo-Rathert et al. (2013)
41.37	67.71	3.75	Calvo-Rathert et al. (2013)
41.37	92.38	3.75	Calvo-Rathert et al. (2013)
41.46	38.58	3.15	Calvo-Rathert et al. (2013)
41.46	68.83	3.15	Calvo-Rathert et al. (2013)
41.48	17.33	3.75	Goguitchaichvili et al. (2009)
41.48	16.65	3.73	Goguitchaichvili et al. (2009)
41.48	11.89	3.71	Goguitchaichvili et al. (2009)
41.48	20.90	3.65	Goguitchaichvili et al. (2009)
41.47	19.71	3.69	Goguitchaichvili et al. (2009)
41.47	23.11	3.67	Goguitchaichvili et al. (2009)
41.47	21.75	3.65	Goguitchaichvili et al. (2009)
41.47	55.06	3.63	Goguitchaichvili et al. (2009)
41.47	38.75	3.61	Goguitchaichvili et al. (2009)
41.47	21.75	3.59	Goguitchaichvili et al. (2009)
Apnia			
41.37	54.63	3.09	This work
41.37	45.59	3.70	This work
41.37	33.70	3.70	This work
41.37	28.58	3.70	This work
41.37	38.67	3.70	This work
41.37	40.92	3.70	This work
41.37	35.73	3.70	This work
41.37	32.99	3.70	This work
Georgia present EMF intensity			
41.37	83.70	0.00	www.ngdc.noaa.gov/geomag

Table S1. VADM calculated from the paleointensities between 3 and 4 Ma (age covered by Apnia sequence) extracted from the PINT2015.05 database (Biggin et al., 2010).

lat (N°)	VADM (ZAm^2)	age (Ma)	references	site
23.0	42.2	3.10	Tauxe (2006)	0474a
-47.0	26.4	2.80	Tauxe (2006)	0862a
-78.2	59.3	2.50	Tauxe et al. (2004a)	mc21
-78.3	52.7	2.50	Tauxe et al. (2004a)	mc30
-78.4	77.9	4.47	Tauxe et al., (2004a)	mc37
45.0	64.9	3.40	Tauxe et al. (2004b)	sr01
-78.2	37.8	2.51	Lawrence et al. (2009)	mc121
-78.2	46.4	4.00	Lawrence et al. (2009)	mc128
-78.2	21.8	4.00	Lawrence et al. (2009)	mc131
-78.2	4.7	4.00	Lawrence et al. (2009)	mc132
-78.2	59.3	4.00	Lawrence et al. (2009)	mc21
-77.2	55.5	2.50	Lawrence et al. (2009)	mc214
-78.3	56.1	4.00	Lawrence et al. (2009)	mc30
-78.4	46.0	4.00	Lawrence et al. (2009)	mc32
-78.4	77.9	4.47	Lawrence et al. (2009)	mc37

Table S2. VADM calculated from the paleointensities between 2.5 and 4.5 Ma extracted from the MagIC database and interpreted by the RCRIT set of selection criteria.

Sánchez-Moreno et al., 2018					This study			Calvo-Rathert et al., 2013		
VGP polarity	directional group	sites	n_{SITE}	age (Ma)	B (μT)	n_{SITE}	σ_{SITE} (μT)	B (μT)	n_{SITE}	σ_{SITE} (μT)
	DG1	AP01-02	2	3.09						
normal	DG2	AP04	1		32.1	5	3.3	54.3	1	2.2
	DG3	AP03-05	2	3.28						
transicional	DG4	AP06	1					26.0	1	1.4
		AP07-10		3.75						
		AP12		3.70						
	DG5	AP11	9		26.8	3	4.0	27.4	2	4.0
		AP13								
		AP14			19.8	8	0.4			
reverse		AP15								
	DG6	AP16	2		16.8	5	2.4	39.8	6	7.8
		AP17			22.7	6	4.3			
	DG7	AP18	3		24.1	5	0.4	17.3	5	1.6
		AP19			21.0	5	0.7	76.1	1	7.7
		AP20			19.4	3	0.0			

Table S3. Paleointensity results from (Calvo-Rathert et al., 2013) correlate with the results from this study by mean of paleomagnetic information and directional groups obtained in (Sánchez-Moreno et al., 2018).

References

Biggin, A. J., McCormack, A., & Roberts, A. (2010). Paleointensity Database Updated and Upgraded. *Eos, Transactions American Geophysical Union*, *91*(2), 15. https://doi.org/10.1029/2010EO020003

Bogue, S.W., Paul, H.A., 1993. Distinctive field behavior following geomagnetic reversals. Geophys. Res. Lett. 20, 2399–2402. doi:10.1029/93GL02473

Calvo-Rathert, M., Bógalo, M.F., Gogichaishvili, A., Sologashvili, J., Vashakidze, G., 2013. New paleomagnetic and paleointensity data from Pliocene lava flows from the Lesser Caucasus. J. Asian Earth Sci. 73, 347–361. doi:10.1016/j.jseaes.2013.04.039

Camps, P., Ruffet, G., Shcherbakov, V.P., Shcherbakova, V. V., Prévot, M., Moussine-Pouchkine, A., Sholpo, L., Goguitchaichvili, A., Asanidzé, B., 1996. Paleomagnetic and geochronological study of a geomagnetic field reversal or excursion recorded in pliocene volcanic rocks from Georgia (Lesser Caucasus). Phys. Earth Planet. Inter. 96, 41–59. doi:10.1016/0031-9201(95)03110-3

Coe, R.S., Gromme, S., Mankinen, E.A., 1984. Geomagnetic paleointensities from excursion sequences in lavas on Oahu, Hawaii. J. Geophys. Res. 89, 1059–1069. doi:10.1029/JB089iB02p01059

Day, R., Fuller, M., & Schmidt, V. A. (1977). Hysteresis properties of titanomagnetites: Grain-size and compositional dependence. *Physics of the Earth and Planetary Interiors*, *13*(4), 260–267. https://doi.org/10.1016/0031-9201(77)90108-X

Dunlop, D. J. (2002). Theory and application of the Day plot (Mrs/Ms versus Hcr/Hc) 1. Theoretical curves and tests using titanomagnetite data. *Journal of Geophysical Research*, *107*(B3), EPM4-1-EPM4-22. https://doi.org/10.1029/2001JB000486

Goguitchaichvili, A., Canon-Tapia, E., Negrete, R., 2003. Paléointensités géomagnétiques absolues complémentaires de la Basse Californie : Évaluation des données du Pliocène et du Pléistocène inférieur et moyen. Comptes Rendus - Geosci. 335, 995–1004. doi:10.1016/j.crte.2003.07.002

Goguitchaichvili, A., Cervantes, M.A., Rathert, M.C., Camps, P., Sologashvili, J., Maissuradze, G.,

2009. Gilbert-Gauss geomagnetic reversal recorded in Pliocene volcanic sequences from Georgia (Lesser Caucasus): Revisited. Earth, Planets Sp. 61, 71–81. doi:10.1186/BF03352886

Herrero-Bervera, E., Valet, J.P., 2005. Absolute paleointensity and reversal records from the Waianae sequence (Oahu, Hawaii, USA). Earth Planet. Sci. Lett. 234, 279–296. doi:10.1016/j.epsl.2005.02.032

Juarez, M.T., Tauxe, L.Y., 2000. The intensity of the time-averaged geomagnetic ¢ eld : the last 5 Myr 175.

Laj, C., Szeremeta, N., Kissel, C., Guillou, H., 2000. Geomagnetic paleointensities at Hawaii between 3.9 and 2.1 Ma: preliminary results. Earth Planet. Sci. Lett. 179, 191–204. doi:10.1016/S0012-821X(00)00098-4

Lawrence, K.P., Tauxe, L., Staudigel, H., Constable, C.G., Koppers, A., McIntosh, W., Johnson, C.L., 2009. Paleomagnetic field properties at high southern latitude. Geochemistry, Geophys. Geosystems 10. doi:10.1029/2008GC002072

Lebedev, V. A., Bubnov, S. N., Dudauri, O. Z., & Vashakidze, G. T. (2008). Geochronology of Pliocene volcanism in the Dzhavakheti Highland (the Lesser Caucasus). Part 1: Western part of the Dzhavakheti Highland. *Stratigraphy and Geological Correlation*, *16*(2), 204–224. https://doi.org/10.1134/S0869593808020081

Sánchez-Moreno, E. M., Calvo-Rathert, M., Goguitchaichvili, A., Vashakidze, G. T., & Lebedev, V. A. (2018). Evidence of Unusual Geomagnetic Regimes Recorded in Plio-Pleistocene Volcanic Sequences from the Lesser Caucasus (Southern Georgia). *Geochemistry, Geophysics, Geosystems*, *19*, 1–18. https://doi.org/10.1029/2017GC007358Morales, J.,

Tauxe, L., 2006. Long-term trends in paleointensity : The contribution of DSDP / ODP submarine basaltic glass collections 156, 223–241. doi:10.1029/2003GC000635

Tauxe, L., Luskin, C., Selkin, P., Gans, P., Calvert, A., 2004. Paleomagnetic results from the Snake River Plain: Contribution to the time-averaged field global database. Geochemistry, Geophys. Geosystems 5. doi:10.1029/2003GC000661

Tauxe, L., Staudigel, H., 2004. Strength of the geomagnetic field in the cretaceous normal superchron: New data from submarine basaltic glass of the troodos ophiolite. Geochemistry, Geophys. Geosystems 5, 223–241. doi:10.1029/2003GC000635

Yamamoto, Y., Tsunakawa, H., 2005. Geomagnetic field intensity during the last 5 Myr: LTD-DHT Shaw palaeointensities from volcanic rocks of the Society Islands, French Polynesia. Geophys. J. Int. 162, 79–114. doi:10.1111/j.1365-246X.2005.02651.x